JASA ARTICLE

Holographic extraction of plane waves from an ultrasound beam for acoustic characterization of an absorbing layer of finite dimensions

Dmitry A. Nikolaev,[1] Sergey A. Tsysar,[1] Vera A. Khokhlova,[1,a)] Wayne Kreider,[2] and Oleg A. Sapozhnikov[1,b)]
[1]*Physics Faculty, Moscow State University, Leninskie Gory, Moscow 119991, Russia*
[2]*Center for Industrial and Medical Ultrasound, Applied Physics Laboratory, University of Washington, 1013 Northeast 40th Street, Seattle, Washington 98105, USA*

ABSTRACT:
For the acoustic characterization of materials, a method is proposed for interpreting experiments with finite-sized transducers and test samples in terms of the idealized situation in which plane waves are transmitted through an infinite plane-parallel layer. The method uses acoustic holography, which experimentally provides complete knowledge of the wave field by recording pressure waveforms at points on a surface intersected by the acoustic beam. The measured hologram makes it possible to calculate the angular spectrum of the beam to decompose the field into a superposition of plane waves propagating in different directions. Because these waves cancel one another outside the beam, the idealized geometry of an infinite layer can be represented by a sample of finite size if its lateral dimensions exceed the width of the acoustic beam. The proposed method relies on holograms that represent the acoustic beam with and without the test sample in the transmission path. The method is described theoretically, and its capabilities are demonstrated experimentally for silicone rubber samples by measuring their frequency-dependent phase velocities and absorption coefficients in the megahertz frequency range. © *2021 Acoustical Society of America*.
https://doi.org/10.1121/10.0003212
(Received 14 September 2020; revised 11 November 2020; accepted 15 December 2020; published online 15 January 2021)
[Editor: Bradley E. Treeby] Pages: 386–404

I. INTRODUCTION

The acoustic properties of media are usually defined by the speed of sound and the attenuation coefficient. These parameters are introduced for a plane harmonic wave with a waveform described as $\exp(-i\omega t + ikz)$, where ω is the angular frequency of the wave, t is time, k is the wavenumber, and z is the coordinate in the direction of wave propagation. Such a wave in its pure form is never realized, in practice, because of the need for unlimited extent in space and time. However, it is customary to consider the behavior of such an idealized wave when characterizing the acoustic properties of propagation media.

The specific properties of the medium are determined by the dispersion law $k = k(\omega)$. The quantity k in the general case is complex, $k = \omega/c + i\,\alpha$. With this expression in mind, the structure of the plane wave takes the form $\exp(-\alpha z)\exp[-i\omega(t - z/c)]$, where c is the phase velocity and α is the wave attenuation coefficient. The dependences, $c = c(\omega)$ and $\alpha = \alpha(\omega)$, and the density, ρ, completely determine the linear acoustic properties of the homogeneous isotropic media.

Since an idealized plane harmonic wave cannot be generated experimentally, in order to measure c and α, conditions are usually created that bring the acoustic field closer to the desired plane-wave form. Experimental determination of the speed of sound and attenuation coefficient is a traditional task of acoustics research. To date, various methods have been developed for measuring these parameters in solids, liquids, and gases. Notably, biological tissues are often considered as a separate type of medium with regard to such characterization methods. A detailed review of relevant work is given in a number of publications, including Refs. 1–3.

Because acoustic waves exhibit a very weak dependence of the phase velocity on frequency, in practice, it is often assumed that there is no dependence, i.e., signals of any waveform propagate at the same speed (speed of sound). In this approximation, the speed of sound measurement does not require a plane harmonic wave but can be performed based on the time delay of a pulsed signal. With such an approach, the speed of sound can be measured with an accuracy on the order of one percent or better using relatively simple experimental configurations.

Measurement of the attenuation coefficient depends more on the structure of the acoustic field and the homogeneity of the medium; therefore, the accuracy of the corresponding measurements is noticeably lower than the

[a)]Also at: Center for Industrial and Medical Ultrasound, Applied Physics Laboratory, University of Washington, 1013 NE 40th Street, Seattle, WA 98105, USA. ORCID: 0000-0002-2585-8228.
[b)]Also at: Center for Industrial and Medical Ultrasound, Applied Physics Laboratory, University of Washington, 1013 NE 40th Street, Seattle, WA 98105, USA. Electronic mail: oleg@acs366.phys.msu.ru

https://doi.org/10.1121/10.0003212

accuracy of the speed of sound measurements. One of the traditional methods for measuring attenuation is the insertion loss method, which involves the introduction of a sample into a reference medium.[4] It is based on a comparison of the amplitudes of two received signals: one is recorded when the test sample is introduced between the source and the receiver, and the other is recorded when there is only a reference medium (e.g., see Ref. 5). To reduce diffraction effects that lead to a strong spatial inhomogeneity of the acoustic field in the near field of typical ultrasonic sources, insertion loss measurements usually employ either a configuration with a small receiver positioned in the far field of the transducer or a flat radiator and a large receiver that are parallel to each other.[6] Although diffraction effects can be partially taken into account by introducing certain correction factors,[7] the accuracy of such measurements is usually low, especially when there are inhomogeneities in the structure of the test material. In addition, the lateral dimension of the sample must exceed several times that of the diameter of both the source and receiver,[6] which is not always possible.

The decay in the amplitude of the propagating plane wave is generally caused by absorption and scattering phenomena, thus, the attenuation coefficient is the sum of the absorption and scattering coefficients. Absorption is caused by the conversion of acoustic energy into heat and, therefore, can be clearly defined. On the contrary, scattering, which occurs only in an inhomogeneous medium, requires more careful consideration. For a plane wave, scattering is defined as the process of converting the energy of the initial wave into the energy of scattered waves propagating in all possible directions, including the original one. This makes it difficult or even impossible to correctly measure the attenuation coefficient.[2] For example, if several plane waves of different directions propagate together, they partly exchange energy due to scattering, then it is impossible to attribute the attenuation coefficient to only one specific plane wave—this coefficient will depend on the presence of waves of other directions. This ambiguity is absent in a homogeneous medium when there is no scattering and the only attenuation mechanism is absorption. Only in this case can the plane wave behave independently of other possible waves. For clarity, in this paper, it is expected that the medium is homogeneous and, hence, the attenuation coefficient coincides with the absorption coefficient.

In the present work, a new approach for measuring the acoustic parameters of various materials is proposed as an extension to the insertion loss method. It is based on the use of acoustic holography, which allows for the experimental recording of complete information about the spatial structure of a wave beam such that the beam can be analytically decomposed into the plane waves it comprises. Consequently, propagation of a beam through a sample of finite lateral dimensions can be interpreted to represent the idealized case of plane wave propagation through an infinite plane-parallel layer of the test material. Due to this possibility, accurate measurements of the acoustic characteristics of materials can be performed.

II. THEORY

A. Transmission of an acoustic beam through a plane-parallel layer

1. Description of the acoustic field in an absorbing medium by the spatial spectrum method

Acoustic pressure $p(\mathbf{r},t)$ in a linear medium can be described by the wave equation

$$\Delta p - \frac{1}{c_i^2}\frac{\partial^2 p}{\partial t^2} + \hat{L}p = 0. \tag{1}$$

Here, $\mathbf{r} = (x,y,z)$ is the position vector of the observation point, t is time, Δ is the Laplace operator, c_i is the speed of sound in the approximation of an ideal medium, and $\hat{L}$ is a linear integrodifferential operator that takes into account the nonideal environment. For example, for a classic viscous fluid $\hat{L} = (b/\rho c_i^2)\Delta\,\partial/\partial t$, where b is the dissipative coefficient that accounts for the viscosity and thermal conductivity, and ρ is the density of the medium.[8]

The solution to Eq. (1) can be obtained using the spectral approach by first representing the wave field $p(\mathbf{r},t)$ as an integral of harmonic signals,

$$p(\mathbf{r},t) = \frac{1}{2\pi}\int_{-\infty}^{\infty} P(\mathbf{r},\omega)e^{-i\omega t}d\omega, \tag{2}$$

where

$$P(\mathbf{r},\omega) = \int_{-\infty}^{\infty} p(\mathbf{r},t)e^{i\omega t}dt. \tag{3}$$

The wave equation (1) for $p(\mathbf{r},t)$ then reduces to the Helmholtz equation for the spectral amplitude $P(\mathbf{r},\omega)$,

$$\Delta P + k^2 P = 0, \tag{4}$$

where k is the wavenumber. The form of the operator $\hat{L}$ determines the dispersion law, i.e., the dependence of the wavenumber on frequency, $k = k(\omega)$. For an ideal fluid, $k = \omega/c_i$.

It is assumed here that a source is present on the plane $z = 0$ and radiates into the half-space $z > 0$. The spectral approach can be further extended to the spatial dependence of $P(\mathbf{r},\omega)$ by calculating the Fourier transform in transverse coordinates (x,y),

$$P(x,y,z,\omega) = \frac{1}{(2\pi)^2}\int_{-\infty}^{\infty}\int_{-\infty}^{\infty} dk_x dk_y S(k_x,k_y,z,\omega) \times e^{i(k_x x + k_y y)}, \tag{5}$$

where integration is carried out over spatial frequencies k_x and k_y. The inverse Fourier transform has the following form:

$$S(k_x,k_y,z,\omega) = \int_{-\infty}^{\infty}\int_{-\infty}^{\infty} dx\,dy\,P(x,y,z,\omega)e^{-i(k_x x + k_y y)}. \tag{6}$$

Taking into account the radiation condition, the Helmholtz equation (4) yields the following solution for the complex amplitude of the spatial spectrum $S(k_x, k_y, z, \omega)$:

$$S(k_x, k_y, z, \omega) = S_0(k_x, k_y, \omega) e^{i\sqrt{k^2 - k_x^2 - k_y^2}\, z}, \tag{7}$$

where, according to Eq. (6),

$$S_0(k_x, k_y, \omega) = \int_{-\infty}^{\infty} \int_{-\infty}^{\infty} dx dy P(x, y, 0, \omega) e^{-i(k_x x + k_y y)}. \tag{8}$$

Taking into account Eq. (7), the spectral decomposition from Eq. (5) takes the following form:

$$P(x, y, z, \omega) = \frac{1}{(2\pi)^2} \int_{-\infty}^{\infty} \int_{-\infty}^{\infty} dk_x dk_y S_0(k_x, k_y, \omega) \times e^{i\left(k_x x + k_y y + \sqrt{k^2 - k_x^2 - k_y^2}\, z\right)}. \tag{9}$$

For the case of an ideal medium when $k = \omega/c_i$ is a real quantity, the wave field represented by Eq. (9) comprises plane waves of the form $e^{i\mathbf{k}\cdot\mathbf{r}}$ in which the corresponding wave vector $\mathbf{k} = (k_x, k_y, k_z = \sqrt{k^2 - k_x^2 - k_y^2})$ for different spatial frequencies (k_x, k_y) has the same length $|\mathbf{k}| = \omega/c_i = \sqrt{k_x^2 + k_y^2 + k_z^2}$ but different inclination angles with respect to the coordinate axes. Therefore, the function $S_0(k_x, k_y, \omega)$ is called the "angular spectrum" when k is real.[9]

In a dissipative medium, the interpretation of solution (9) as a superposition of plane waves requires more careful consideration. In this case, as previously noted, $k = \omega/c + i\alpha$ is already a complex quantity and, hence, the axial component of the wave vector $k_z = k'_z + ik''_z$ is also complex. As a result, elementary waves acquire a structure $e^{-k''_z z} e^{i(k_x x + k_y y + k'_z z)}$ and, thus, cannot be considered to be obliquely propagating plane waves that decay. Moreover, they can be called "plane waves" with a caveat: surfaces of equal phase are one family of planes, $k_x x + k_y y + k'_z z = \text{const}$, and surfaces of equal amplitude are another family, $z = \text{const}$.

The question then arises of whether it is possible to use "real" plane waves of the form $e^{i\mathbf{k}\cdot\mathbf{r}}$ propagating in different directions as the basic functions of spatial spectral decomposition for the wave field in a dissipative medium. The answer to this question is negative because for such waves, it becomes impossible to set a boundary condition on the plane $z = 0$. Indeed, for a decaying plane wave propagating along a unit vector $\mathbf{m}$, the wave vector is $\mathbf{k} = k\mathbf{m} = (\omega/c + i\alpha)\mathbf{m}$. It follows that on the plane $z = 0$, the amplitude of the indicated wave is proportional to $e^{-\alpha(m_x x + m_y y)}$, i.e., it grows indefinitely along the radiating surface $z = 0$ as $m_x x + m_y y \to -\infty$. For an ideal medium without dissipation, the solution (9) representing an angular spectrum with a real wavenumber is free from this drawback and is, therefore, suitable for the analysis of a wave field of arbitrary form.

In general, the expression (9) means that the total field is represented as a superposition of transverse modes of the form $e^{i(k_x x + k_y y)}$ propagating along the axis z. The propagation constant (wavenumber) of each of these modes, $k_z = \sqrt{k^2 - k_x^2 - k_y^2}$, depends on the dispersion law $k = k(\omega)$ and spatial frequencies (k_x, k_y). The field in a non-dissipative medium, such as water, can be represented by a superposition of true plane waves (an angular spectrum), which is a particular case of Eq. (9). However, the field within an absorptive layer will possess a more general wave structure. In Sec. II A 2, a method for characterizing the wave propagation in an absorptive layer is developed based on angular spectra that describe the field entering and leaving the layer.

2. Transmission through a plane-parallel layer oriented perpendicular to the z axis

Let us consider the situation when a plane-parallel layer of thickness H, made from the test material, is placed in the reference medium. Assuming ideal alignment, the flat surfaces of this layer are perpendicular to the axis z, intersecting it at points $z_0 > 0$ and $z_0 + H$. At a point with a coordinate $z > z_0 + H$, in the absence of the layer, the spectral amplitude is expressed from Eq. (7) as

$$S_{\text{without layer}}(k_x, k_y, z, \omega) = S_0(k_x, k_y, \omega) e^{i\sqrt{k_0^2 - k_x^2 - k_y^2}\, z}. \tag{10}$$

In the presence of a layer,

$$S_{\text{with layer}}(k_x, k_y, z, \omega) = S_0(k_x, k_y, \omega) e^{i\sqrt{k_0^2 - k_x^2 - k_y^2}\, z_0} \times T_{\text{in}} e^{i\sqrt{k^2 - k_x^2 - k_y^2}\, H} \times T_{\text{out}} e^{i\sqrt{k_0^2 - k_x^2 - k_y^2}\, (z - z_0 - H)}, \tag{11}$$

where $k_0(\omega)$ and $k(\omega)$ are the wavenumbers in the reference and test media, respectively, and T_{in} and T_{out} are the transmission coefficients for the beam entering from the reference medium into the layer and exiting from the layer into the reference medium, respectively.

Equation (11) assumes that the layer is thick enough that multiple reflections within the layer do not contribute to the transmitted wave. As a rule, the transmitted wave is a superposition of a series of multiply reflected waves, therefore, instead of Eq. (11), one should use the well-known expression for the coefficient of transmission through the layer in the continuous wave (CW) mode.[10] Although this approach is possible (the corresponding expressions are somewhat more cumbersome but also straightforward), it is assumed below that the first transmitted wave is separated from its multiple reflections in time. In practice, this separation can be performed in the pulsed regime if the layer thickness is large enough so that the re-reflected waves can be separated from the first transmitted signal in time, that is, this signal is shorter than the corresponding delay, $2H/c$. This approach is used below.

The ratio of the angular spectra measured in the same place in the absence of the layer and with the layer does not

https://doi.org/10.1121/10.0003212

depend on its position z_0, the initial amplitude of the angular spectrum S_0, or the coordinate of the measurement z; this ratio depends only on the thickness and acoustic properties of the layer

$$\Pi(k_x,k_y,\omega)=\frac{S_{\text{with layer}}(k_x,k_y,z,\omega)}{S_{\text{without layer}}(k_x,k_y,z,\omega)}=T_{\text{in-out}}(k_x,k_y,\omega)\,e^{i\left(\sqrt{k^2-k_x^2-k_y^2}-\sqrt{k_0^2-k_x^2-k_y^2}\right)H}, \tag{12}$$

where $T_{\text{in-out}}=T_{\text{in}}T_{\text{out}}$ is the total transmission coefficient that accounts for losses at the layer interfaces. The value $T_{\text{in-out}}=T_{\text{in-out}}(k_x,k_y,\omega)$ is based on the continuity condition of the normal components of the tensor of mechanical stresses and vibrational velocity and can be expressed in terms of the effective impedances for the corresponding mode in the test layer and the reference medium,

$$T_{\text{in-out}}=\frac{4Z_0Z}{(Z_0+Z)^2}, \tag{13}$$

$$Z_0=\rho_0\omega/\sqrt{k_0^2-k_x^2-k_y^2}, \tag{14}$$

$$Z=\rho\omega/\sqrt{k^2-k_x^2-k_y^2}, \tag{15}$$

where the "0" subscripts and no subscripts refer to properties of the reference medium and properties of the test layer, respectively. For modes with nonzero spatial frequencies, which correspond to an inclined incidence of the wave relative to the layer, there are also additional losses at the interfaces caused by the excitation of viscous waves. Such waves correspond to the vortex mode of motion of a continuous medium rather than the acoustic one.[11] However, these additional losses can be neglected for relatively small incidence angles ($k_x^2+k_y^2\ll k_0^2$) and viscosities. We also note that in the absence of absorption, Eq. (13) is a well-known expression for the coefficient of transmission through a layer by means of "normal impedances," equal to the ratio of the corresponding "characteristic impedances" of the media to the cosines of the angles of incidence and refraction, $Z_0=\rho_0c_0/\cos\theta_0$ and $Z=\rho c/\cos\theta$, where $\theta_0=\arcsin(\sqrt{k_x^2+k_y^2}/k_0)$ and $\theta=\arcsin(\sqrt{k_x^2+k_y^2}/k)$.

The function $\Pi(k_x,k_y,\omega)$ has the meaning of a propagator for the corresponding component of the angular spectrum. We use the following representation:

$$\Pi(k_x,k_y,\omega)=A_\Pi(k_x,k_y,\omega)e^{i\Phi_\Pi(k_x,k_y,\omega)}, \tag{16}$$

where A_Π and Φ_Π are real quantities representing the magnitude and phase of the propagator, respectively. Because in Eq. (12), k and $T_{\text{in-out}}$ are complex quantities, the expressions for A_Π and Φ_Π are rather cumbersome. To simplify them, we will consider a case of practical interest for which nontrivial wave absorption occurs at a distance much greater than a wavelength. Then, in the expression for the wavenumber $k=\omega/c+i\alpha$ in the absorbing layer, the imaginary part is much smaller than the real one, $\alpha c/\omega\ll 1$. Neglecting terms above first order in the small parameter $\alpha c/\omega$, we obtain

$$A_\Pi(k_x,k_y,\omega)\approx\hat{T}_{\text{in-out}}\exp\left[-\omega H\left(\frac{\alpha/c}{\sqrt{(\omega/c)^2-k_x^2-k_y^2}}-\frac{\alpha_0/c_0}{\sqrt{(\omega/c_0)^2-k_x^2-k_y^2}}\right)\right], \tag{17}$$

$$\Phi_\Pi(k_x,k_y,\omega)\approx\left(\sqrt{(\omega/c)^2-k_x^2-k_y^2}-\sqrt{(\omega/c_0)^2-k_x^2-k_y^2}\right)H+\frac{\hat{Z}-\hat{Z}_0}{\hat{Z}+\hat{Z}_0}\left(\frac{\alpha\omega/c}{(\omega/c)^2-k_x^2-k_y^2}-\frac{\alpha_0\omega/c_0}{(\omega/c_0)^2-k_x^2-k_y^2}\right). \tag{18}$$

Here, $\alpha_0=\alpha_0(\omega)$ is the absorption coefficient in the reference medium, which is assumed to be known. Also,

$$\hat{Z}_0=\frac{\rho_0c_0}{\sqrt{1-(k_x^2+k_y^2)/(\omega/c_0)^2}} \tag{19}$$

and

$$\hat{Z}=\frac{\rho c}{\sqrt{1-(k_x^2+k_y^2)/(\omega/c)^2}} \tag{20}$$

are normal impedances of the media [see Eqs. (14) and (15)] with neglect of absorption, and

$$\hat{T}_{\text{in-out}}=\frac{4\hat{Z}_0\hat{Z}}{(\hat{Z}_0+\hat{Z})^2} \tag{21}$$

is the corresponding transmission coefficient through two interfaces.

For a mode that corresponds to zero spatial frequencies $k_x=k_y=0$, the expressions can be simplified. In this case, the mode itself is a plane wave propagating perpendicular to the layer, and Eqs. (17) and (18) take the following forms:

$$A_\Pi(0,0,\omega)=\frac{4\rho_0c_0\rho c}{(\rho_0c_0+\rho c)^2}\exp\left[-(\alpha-\alpha_0)H\right], \tag{22}$$

$$\Phi_\Pi(0,0,\omega)=\left(\frac{1}{c}-\frac{1}{c_0}\right)\omega H+\frac{\alpha c-\alpha_0c_0}{\omega}\frac{\rho c-\rho_0c_0}{\rho c+\rho_0c_0}. \tag{23}$$

Estimates show that under the conditions of the experiment described below, the second term in Eq. (23) makes a few orders of magnitude smaller contribution to the phase

change compared with the first term and, therefore, it can be neglected. Then the algorithm for measuring the phase velocity and absorption coefficient is simplified and reduced to two steps. At the first step, the phase velocity is calculated from the propagator phase Φ_Π, defined by Eq. (23),

$$\frac{1}{c(\omega)} = \frac{1}{c_0(\omega)} + \frac{\Phi_\Pi(0,0,\omega)}{\omega H}. \tag{24}$$

After that, taking into account Eq. (22), the absorption coefficient is expressed from the propagator magnitude $A_\Pi(0,0,\omega)$,

$$\alpha(\omega) = \alpha_0(\omega) + \frac{1}{H}\left[\ln\left(\frac{4\rho_0 c_0 \rho c}{(\rho_0 c_0 + \rho c)^2}\right) - \ln A_\Pi(0,0,\omega)\right]. \tag{25}$$

Thus, to solve the problem of finding the phase velocity $c(\omega)$ and the absorption coefficient $\alpha(\omega)$, it is sufficient to use only the propagator $\Pi(0,0,\omega)$.

It is convenient to choose water as a reference medium. For water, the dispersion of the phase velocity can be neglected, and the absorption ($\alpha_0/f^2 \approx 2.5 \times 10^{-14}\text{s}^2/\text{m}$, $f = \omega/2\pi$) can be also considered negligible compared to the absorption in the test medium.[12,13] Based on this assumption, the speed c_0 is considered to be independent of the frequency, and the absorption is considered to be absent, $\alpha_0 = 0$.

The propagator $\Pi(0,0,\omega)$ sets the complex amplitude of a plane wave after passing through the test layer in the case when the initial wave amplitude is equal to unity. Therefore, its Fourier transform,

$$g(t) = \frac{1}{2\pi}\int_{-\infty}^{\infty} \Pi(0,0,\omega) e^{-i\omega t} d\omega, \tag{26}$$

represents the impulse response, that is, the waveform at the output of the layer when the acoustic disturbance in the form of the Dirac delta function $\delta(t)$ is specified at the input to the layer. Due to the peculiarities of measuring holograms (using the method of replacing a layer with a reference medium), the impulse response is additionally shifted in time by an amount H/c_0, corresponding to the passage time of a layer of the reference medium of the same thickness. To find $g(t)$, it is necessary to expand the domain of the propagator definition to negative frequencies according to the rule $\Pi(0,0,\omega) = \Pi^*(0,0,-\omega)$, where the star means complex conjugation. In practice, the propagator is known only in a limited frequency band; therefore, the corresponding Fourier image found by integration over a finite frequency interval will differ slightly from the exact impulse response.

3. Use of the propagator values at different spatial frequencies as a statistical ensemble to improve the accuracy of estimated properties

At first glance, it might seem that in relation to the problem under consideration, the holography method gives unnecessary redundant data, which are propagators $\Pi(k_x, k_y, \omega)$ for a large number of nonzero spatial frequencies (k_x, k_y). However, such a conclusion is valid only in the ideal case when $\Pi(0,0,\omega)$ is measured absolutely accurately. When finding $c(\omega)$ and $\alpha(\omega)$ in a real experiment, inevitable errors appear due to uncertainty in measuring holograms. These errors can be reduced if a large number of statistically independent measurements are performed and the resulting values are averaged over the statistical ensemble. Propagators $\Pi(k_x, k_y, \omega)$ provide such an opportunity. Indeed, propagators for different (k_x, k_y) can be considered independent quantities, and each of them contains information about the parameters $c(\omega)$ and $\alpha(\omega)$. To describe the specified statistical ensemble, we mark the implementation of random variables $c(\omega)$ and $\alpha(\omega)$, found from the propagator $\Pi(k_x, k_y, \omega)$, with superscripts: $c^{(k_x,k_x)}(\omega)$ and $\alpha^{(k_x,k_x)}(\omega)$. Equations (24) and (25) give an expression for $c^{(0,0)}(\omega)$ and $\alpha^{(0,0)}(\omega)$. Equations (17) and (18) make it possible to use the experimental measurement of the complex quantity $\Pi(k_x, k_y, \omega)$ to find $c^{(k_x,k_x)}(\omega)$ and $\alpha^{(k_x,k_x)}(\omega)$. Since these quantities are included in both Eqs. (17) and (18), in practice, it is convenient to find them by the method of successive approximations. In a first approximation, absorption can be neglected in the estimation of the phase velocity in the test layer from Eq. (18) for the propagator phase. Using this estimate, the absorption coefficient can be readily calculated from Eq. (17) for the propagator magnitude A_Π. These initial estimates can then be improved iteratively by using the current estimate of the absorption coefficient to recalculate the phase velocity from Eq. (18) and the new sound speed value to recalculate the absorption coefficient from Eq. (17).

For convenience, we note that Eqs. (17) and (18) look relatively simple at small frequencies for which the condition $k_x^2 + k_y^2 \ll k_0^2$ is met. Up to terms quadratic in spatial frequencies, the phase velocity and absorption coefficient are expressed in terms of the propagator magnitude and phase as

$$\frac{1}{c^{(k_x,k_y)}(\omega)} \approx \frac{1}{c_0} + \frac{\Phi_\Pi(k_x,k_y,\omega)}{\omega H}\left[1 - \frac{c_0 c}{2\omega^2}\left(k_x^2 + k_y^2\right)\right], \tag{27}$$

$$\alpha^{(k_x,k_y)}(\omega) \approx \alpha^{(0,0)}(\omega) + \frac{1}{H}\left\{\ln\left[\frac{A_\Pi(0,0,\omega)}{A_\Pi(k_x,k_y,\omega)}\right] + \frac{(c^2 - c_0^2)(\rho_0 c_0 - \rho c)}{2\omega^2(\rho_0 c_0 + \rho c)}\left(k_x^2 + k_y^2\right)\right\}. \tag{28}$$

Considering the right-hand side of Eqs. (27) and (28), c can be approximated by the value $c^{(0,0)}$ as found by Eq. (24) if errors on the order of $\sim(k_x^2 + k_y^2)$ are neglected. After finding $c^{(k_x,k_y)}(\omega)$ and $\alpha^{(k_x,k_y)}(\omega)$ for all considered spatial frequencies, an averaging operation should be carried out to provide much more accurate estimates of c and α than could be achieved through the use of only the propagator $\Pi(0,0,\omega)$.

https://doi.org/10.1121/10.0003212

Up to this point, we have assumed that the incident beam as measured by a three-coordinate positioner (see below) is well aligned with the test sample so that the positioner's z axis is perpendicular to the test layer. Consequently, the propagator evaluated at zero frequencies corresponds to a plane wave at normal incidence to the layer. However, this alignment may not be achieved in practice. As explained in detail in Appendix A, modified expressions for the propagator should be used to account for such misalignments.

4. Determination of the absorption coefficient based on the total acoustic power transmitted through a layer for a beam with a narrow angular spectrum

The method for finding acoustic characteristics described above is based on the fact that after passing through a plane-parallel homogeneous layer, a plane wave does not change its structure, i.e., remains a plane wave with the same direction of propagation. In practice, the condition of plane parallelism and uniformity of the layer cannot always be ensured. In this case, the representation of the wave field as a superposition of noninteracting plane waves of different directions is not possible. At each distance z, one can still use expansion (5) and assume that a superposition of the transverse modes of the form $e^{i(k_x x+k_y y)}$ is given in the corresponding transverse plane. In the presence of heterogeneity at an infinitely small step $z \rightarrow z+dz$, each of these modes is generally distorted and thereby generates a set of new modes with different spatial frequencies. In other words, the heterogeneity of the medium leads to the interaction of the components of the spatial spectrum. It is important, however, that with a weak and smooth inhomogeneity, each transverse mode gives rise to modes with close spatial frequencies. In particular, if a wave beam incident on a layer has a spatial spectrum localized near zero frequency $(k_x, k_y) = (0, 0)$, then as a result of mode mixing caused by weak inhomogeneities, the beam will retain this localization property near zero frequency at all stages of propagation. Since at a small step $z \rightarrow z+dz$, the mixing of the modes due to the inhomogeneity does not change the total power of the wave, $W(z,\omega)$, and the dissipation of each mode occurs according to the law of absorption of a plane wave, we can assume that the dependence of the total power on distance is described by the same formula as for a plane wave, $W(z,\omega) \sim e^{-2\alpha(\omega)z}$. It follows that the beam power in the absence of a layer, $W_{\text{without layer}}$, and the beam power in the presence of a layer, $W_{\text{with layer}}$, are related as follows:

$$\frac{W_{\text{with layer}}(z,\omega)}{W_{\text{without layer}}(z,\omega)} = \left(T^{(0)}_{\text{in-out}}\right)^2 e^{-2\alpha(\omega)H}. \tag{29}$$

Here, we introduce a notation for the transmission coefficient of a plane wave through the boundaries of the layer during normal incidence

$$T^{(0)}_{\text{in-out}} = \frac{4\rho_0 c_0 \rho c}{(\rho_0 c_0 + \rho c)^2}. \tag{30}$$

Therefore, the absorption coefficient can be found by measuring the total beam power

$$\alpha(\omega) = \frac{1}{2H}\left\{\ln\left[\frac{W_{\text{without layer}}(z,\omega)}{W_{\text{with layer}}(z,\omega)}\right] + 2\ln T^{(0)}_{\text{in-out}}\right\}. \tag{31}$$

It is noteworthy that the values of the total beam power included in this formula are quite simply expressed through the angular spectrum of the wave[14]

$$W(z,\omega) = \frac{1}{8\pi^2\rho_0 c_0}\iint_{k_x^2+k_y^2\le k_0^2} dk_x dk_y \times \sqrt{1-\frac{k_x^2+k_y^2}{k_0^2}}\,|S(k_x,k_y,z,\omega)|^2. \tag{32}$$

The spatial spectrum included here, as noted above, can be determined from the experimentally measured hologram. Thus, Eqs. (30) and (31) make it possible to extend the holographic method of measuring the absorption coefficient to the case of weak inhomogeneity. It is important to recall that the use of the described approach gives only an approximate value for the absorption coefficient, which will be more accurate for beams with narrower angular spectra.

B. Finding the angular spectrum of an acoustic field based on its hologram

According to Eq. (9), the acoustic field at any point in space is completely determined by its angular spectrum $S_0(k_x, k_y, \omega)$, which is the Fourier transform of the surface distribution of the complex amplitude of the acoustic pressure at the source, $P(x, y, 0, \omega)$. From Eqs. (6) and (7), it follows that the spectrum $S_0(k_x, k_y, \omega)$ can be calculated on the basis of the transverse distribution of the pressure amplitude not only on the source plane $z = 0$ but also on any other plane $z = z_H$

$$S_0(k_x,k_y,\omega) = e^{-i\sqrt{k^2-k_x^2-k_y^2}\,z_H} \times \int_{-\infty}^{\infty}\int_{-\infty}^{\infty} dx dy P(x,y,z_H,\omega) e^{-i(k_x x+k_y y)}. \tag{33}$$

The two-dimensional transverse distribution $P(x, y, z_H, \omega)$ is, hence, a complete record of the wave field $P(x, y, z, \omega)$, i.e., its hologram.[15,16]

Although, formally, the support of the transverse coordinate function $P(x, y, z_H, \omega)$ is the entire infinite coordinate plane (x, y), for a large source, as compared to a wavelength, the acoustic field is a wave beam bounded in the transverse direction. Therefore, we can assume that the specified beam crosses a portion of a finite size comparable to the diameter of the source. In addition, when moving away from the source, the evanescent components of the angular spectrum decay and, therefore, the beam consist only of propagating components whose frequencies satisfy the condition

$k_x^2 + k_y^2 \leq k_0^2$. According to the Nyquist criterion, a function with a limited spectrum is completely determined by its discrete values at the nodes of the spatial grid, the step of which does not exceed half the wavelength. This leads to an important practical conclusion that to record a hologram, it is sufficient to measure the magnitude and phase of the wave in a limited number of points on a surface area that intersects the wave beam. It is convenient to place these points in the nodes of the square grid.

Since the step of such a grid should be half the wavelength or less, for large (compared to the wavelength) sources, the required number of recording points can be significant. For example, for centimeter-sized sources operating in water in the megahertz frequency range, the size of the hologram is on the order of 100×100 pixels. Ultrasonic receiving devices with such a large number of elements do not exist yet, but this problem is bypassed by synthesizing a two-dimensional array of receivers using a single receiver, sequentially placed in nodes of the synthesized array. In practice, this hologram registration process is automated using computer-controlled positioning systems.[15]

As mentioned, the analysis of the spatial spectrum of an acoustic beam transmitted through a plane-parallel layer of the test medium allows one to determine the acoustic properties of the layer. Since the propagator specified by Eq. (12) does not depend on the specific form of the spatial spectrum, the result is valid for any beam, including a beam of small diameter, for example, the one radiated by a miniature source. This means that, in practice, a plane-parallel layer infinite in the transverse direction is not needed; it can be replaced only by its portion in which the acoustic beam is present. In other words, the idealized process of the passage of a plane wave through an infinite plane-parallel layer can be indirectly implemented using a narrow beam and a small sample. This conclusion is important for practice because it allows one to exclude the influence of diffraction on the process of measuring the acoustic characteristics of the test material.

III. EXPERIMENT

The method described in Sec. II for measuring the absorption coefficient and phase velocity is suitable for waves of any nature. To illustrate its performance, an experiment was carried out with ultrasound in the megahertz range with relevance to medical applications and nondestructive testing of materials. More specifically, the purpose of the experiment was to validate the applicability of the method for layers with a limited transverse size, as well as to demonstrate the ability of the method to achieve high measurement accuracy by using averaging over a statistical ensemble formed by plane waves of different directions corresponding to the angular spectrum of the wave beam.

A. Materials and methods

1. Test samples for measuring acoustic properties

Plane-layered samples made of room-temperature-vulcanizing silicone rubber (RTV-2, Wacker Chemie AG, Munich, Germany) were used in the experiments. Such RTV materials, due to their stability, are commonly used as phantoms of soft biological tissues even though they have a slightly lower speed of sound and higher absorption.[17]

To prepare the samples, the liquid mixture from the rubber base and hardener was poured into one of several containers. For disk-shaped samples, each container was fabricated from a section metal pipe cut on a lathe in conjunction with a glass plate pressed to each end of the pipe section. This ensured a high degree of parallelism and smoothness of the plane surfaces of the samples. A hole was drilled in the pipe wall to facilitate filling of the container with the glass plates in place. Samples were degassed by placing the container in a vacuum desiccator for several hours until the rubber solidified completely. The diameters of the disk-shaped samples were equal to the inner diameter of the pipe (108 mm), and the thicknesses corresponded to different pipe-section lengths. In addition, a rectangular cuboid-shaped sample with the thickness of the thickest disk but much smaller transverse dimensions was manufactured using a similarly machined container. Figure 1 shows a photograph of a disk-shaped and a cuboid-shaped sample; the dimensions of all samples are listed in Table I. The uncertainty of the thickness of the layers (± 0.05 mm) was estimated based on ten measurements of the thickness at different points of each sample using a micrometer screw gauge with an accuracy of 0.01 mm. The density of the rubber was determined to be $1196 \pm 27\ \mathrm{kg/m^3}$ based on measurements of sample weights and dimensions.

2. Experimental setup

The arrangement of the main elements of the experimental setup is illustrated in Fig. 2. An ultrasonic field in the form of a focused beam was created in water by a piezoelectric transducer with a nominal diameter of 38.1 mm, focal length of 63.5 mm, and center frequency of 1 MHz (V392, Panametrics, Waltham, MA, USA). The transducer was powered by an electric voltage supplied from a generator (33250A, Agilent, Santa Clara, CA, USA).

The test sample was positioned opposite the source in the prefocal region. The exact location of the sample relative

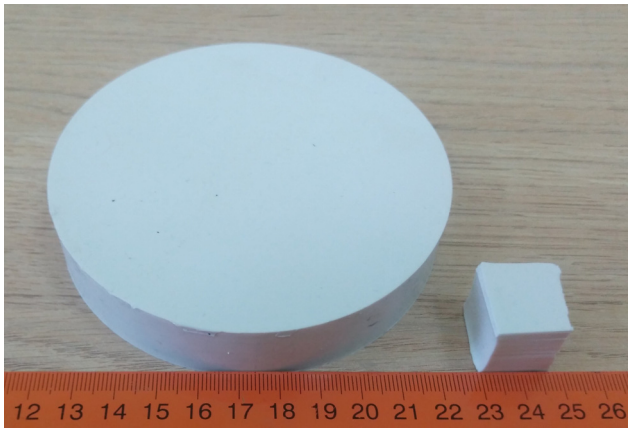

FIG. 1. (Color online) Photograph of samples D20 and C20.

https://doi.org/10.1121/10.0003212

TABLE I. Geometric characteristics of silicone rubber samples used in the experiments.

Sample name	Shape	Thickness (mm)	Cross-sectional size (mm)
D10	Disk	9.68 ± 0.05	Diameter 108
D15	Disk	14.62 ± 0.05	Diameter 108
D20	Disk	19.55 ± 0.05	Diameter 108
C20	Cuboid	19.55 ± 0.05	20×17

to the transducer is not important because the axial position z_0 does not appear in any of the relevant equations defining the propagator per Eq. (12). In practice, the sample was positioned such that the beam width incident on the sample was small relative to the sample size while ensuring that the sample holder did not interfere with the scanning of the hydrophone. Given the transducer's focal length of 63.5 mm and the sample thickness of 10–20 mm, a suitable position was found to approximately correspond to an axial position of $z_0 + H = 46$ mm. This distance was determined with an uncertainty of about 1 mm by placing the needle hydrophone at the acoustic focus and then using the motorized positioner to move the hydrophone near the distal face of the sample as a distance-measuring probe.

The acoustic signal was received by a needle-type hydrophone (HNA-0400, Onda, Sunnyvale, CA, USA) with a sensor diameter of 0.4 mm. The hydrophone was connected to an oscilloscope (TDS5034B, Tektronix, Beaverton, OR, USA) through a preamplifier. The sensitivity at the output of the preamplifier at a frequency of 1 MHz was 8.12×10^{-7} V/Pa.

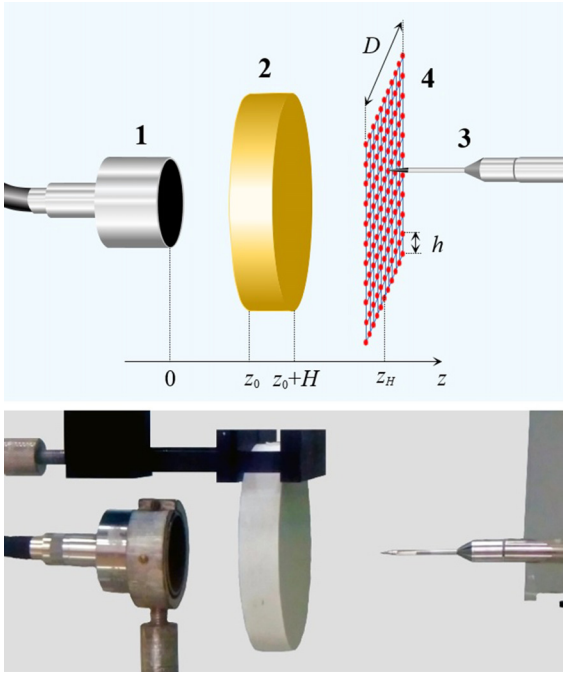

FIG. 2. (Color online) The arrangement used for acoustic measurements. The main elements of the setup are shown at top. (1) Source, (2) test sample, (3) needle hydrophone, and (4) scan area when recording a hologram. Dots indicate positions of the hydrophone during the measurement process. Underneath is a corresponding photograph.

Note that in the considered approach, all measurements are relative; therefore, the amplitude and phase responses of the hydrophone do not play a role, i.e., an uncalibrated hydrophone can be used. The acoustic hologram was measured on a plane perpendicular to the beam axis and located at a distance of 10 mm beyond the focal point at a $z_H = 73.5$ mm.

The hydrophone was successively translated to the nodes of the square grid using a positioning system (UMS-3, Precision Acoustics, Dorchester, UK), which allowed the ultrasound receiver to be moved in three mutually perpendicular directions with a positioning accuracy of 5 μm. The system was controlled using a commercial LabVIEW program (UMS3 Software, Precision Acoustics). The measurements were carried out in a tank $1 \times 0.5 \times 0.5$ m in size, filled with degassed water at a temperature of 24 °C. At this temperature, the density of water is 997 kg/m^3 and the speed of sound is 1496 m/s.[18]

3. Measurement and processing of a time-domain signal at a given point in space

To measure the acoustic parameters at different frequencies, a pulsed mode of operation was used in which an electric voltage $U(t)$ in the form of a tone burst, consisting of a small number of sinusoidal cycles, was applied to the transducer. In most of the measurements described below, the driving electrical signal had an amplitude of 5 V, consisting of three cycles of a 1 MHz sinusoid. This tone burst signal was repeated at a frequency of 100 Hz.

When measuring the hologram at each point of the scanning area, a pulse signal detected by the hydrophone was recorded. To reduce noise, the recorded signals were averaged over 64 realizations. Then, the direct current (DC) component of the received signal (i.e., its average value over time) was subtracted. Each averaged signal scaled by the hydrophone sensitivity yields an acoustic waveform $p(\mathbf{r}, t)$. As described below, time-domain measurements at many scan points were processed to identify spectral components $P(\mathbf{r}, \omega)$ and construct holograms of the acoustic field at various frequencies.[19,20]

Because the signals recorded in the experiment are sampled both in time and space, discrete versions of the Fourier transforms from Eqs. (3) and (6) were employed. This procedure required the choices of spatial and temporal windows within which the signal was recorded and sampling steps. The choice of a window corresponds to the periodization of the analyzed signal, which, in turn, determines a discrete set of frequencies corresponding to harmonics of the Fourier series. The related details are presented in Appendix B. Note that due to the finite time window, the cyclic frequency is changed with the sampling step $\Delta\omega = 2\pi/T$ [see Eq. (B2)], where T is the time-window duration.

Figure 3 shows a typical transducer voltage signal $U(t)$ and corresponding hydrophone signals $u(t) \sim p(\mathbf{r}, t)$ measured at several points on the plane of the hologram. The initial part of the hydrophone signal in each waveform contains an electromagnetic interference pulse, which is almost independent of the position of the measurement point

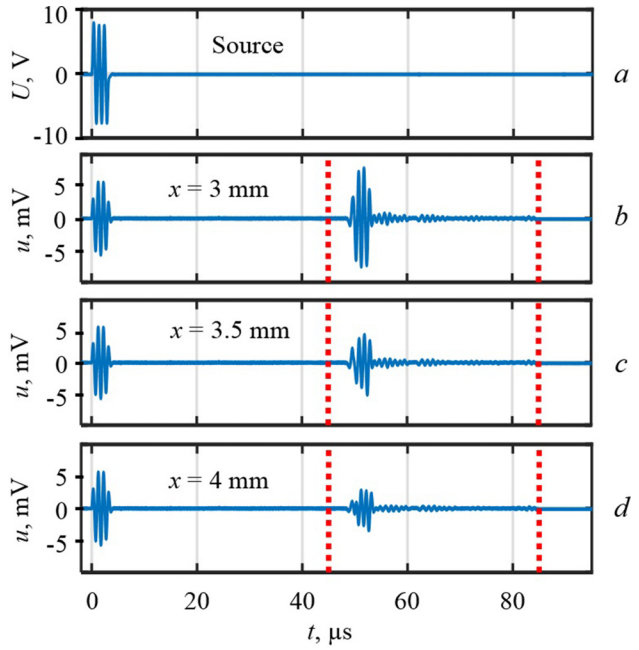

FIG. 3. (Color online) The signal $U(t)$ (a) supplied to the transducer and the corresponding response $u(t)$ of the hydrophone, measured in water (no sample) at various points on the hologram plane [(b)–(d)] at the distance from the source, $z = 73.5$ mm. The signals [(b)–(d)] correspond to distances of 3, 3.5, and 4 mm from the beam axis in the transverse direction, respectively. Vertical dashed lines indicate the boundaries of the time window used when recording acoustic signals.

because it is not associated with acoustic processes. The subsequent impulse in each waveform represents an acoustic signal that is delayed in time relative to the start of radiation. As shown in Fig. 3, whereas the shape of the acoustic signal is similar to the shape of the electrical signal $U(t)$ that feeds the transducer, it does not coincide with it and depends on the position of the hydrophone. These differences can be explained not only by distortions arising in the process of electro-acoustic conversion in a piezoelectric transducer but also by the propagation effects of diffraction and, in the presence of an absorbing layer, the dispersion and absorption of the acoustic wave.

Electromagnetic interference arising before the arrival of the acoustic signal and possible reverberation signals arising after the end of the acoustic pulse were cut off by a suitable choice of the time window. The beginning of the window t_0 was chosen at a time immediately preceding the arrival time of the signal front when the hydrophone was positioned on the beam axis. It is advisable to set t_0 a little earlier than the observed time of arrival of the acoustic signal front, for example, by an amount on the order of several cycles at the central radiation frequency so as not to miss the start of the signal. The window duration T should be chosen sufficiently large so that it contains the entire acoustic signal with its decaying tail. At the same time, the window should end before the arrival of signals associated with acoustic reflections from structural elements and the walls of the water tank.

Based on the above recommendations, for measurements in water using the experimental arrangements of this study, the start of the window was selected at $t_0 = 44.75\ \mu$s. When layers were present, an additional delay (on the order of several microseconds) was introduced, taking into account the difference in the speed of sound in water and in the material of the layers. The window duration was chosen equal to $T = 40\ \mu$s, which made it possible to record the entire pulse signal and cut off the reverberation signals (Fig. 3). According to Eq. (B2), for the chosen value of T, the frequency sampling step was $\Delta f = \Delta\omega/(2\pi) = 25$ kHz. The time sampling step was $h_t = 8$ ns, and the corresponding number of the waveform points was $N = T/h_t = 5000$.

Figure 4 shows the dependence of the absolute value of the spectral amplitude $|P(\mathbf{r}, \omega)|$ on the frequency $f = \omega/(2\pi)$ calculated using Eq. (33) for the hydrophone signal measured at the point of $x = 3$ mm, $y = 0$, $z = 73.5$ mm [see Fig. 3(b)]. It can be seen that the spectral amplitude far exceeds the noise level in a relatively wide frequency range from about 0.4 to 1.6 MHz, which includes approximately 50 frequency points of the discrete spectrum.

4. Angular spectrum at different frequencies obtained from the acoustic hologram

The complex amplitudes of the frequency components $P(\omega, \mathbf{r})$ are functions of spatial coordinates. Similar to the time sampling procedure described above with respect to a signal measured at a given point, the signal is also sampled by transverse spatial variables when scanning the field with a hydrophone. The spatial step when recording the hologram was $h = 0.5$ mm. More details are provided in Appendix B.

Figure 5 shows the transverse distribution of the magnitude and phase of the hologram $P(\mathbf{r}, \omega)$ at one of the frequencies $f = \omega/(2\pi) = 1$ MHz as well as the magnitude and phase of the corresponding angular spectrum calculated using Eq. (B5). When processing experimental data, the indicated values were calculated for all temporal frequencies from a discrete set shown in Fig. 4. From the pattern of the spatial spectrum, it is possible to conclude that although the spectrum is localized near the origin $(k_x, k_y) = (0, 0)$, it is quite wide, i.e., the ultrasound beam contains plane waves of many directions.

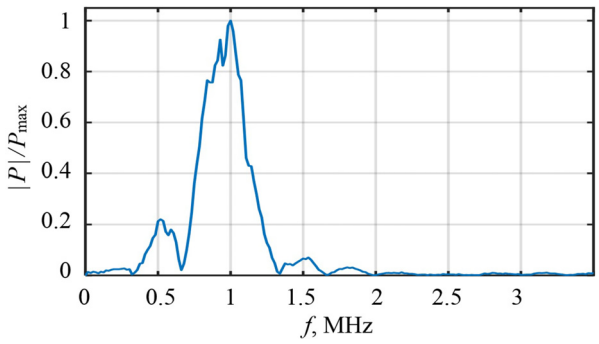

FIG. 4. (Color online) The dependence of the spectral amplitude $|P|$ normalized to its maximum $P_{\max}$ on the frequency for the hydrophone signal at the point $(x, y, z) = (3\text{ mm}, 0, 73.5\text{ mm})$. The corresponding time signal is shown in Fig. 3(b).

https://doi.org/10.1121/10.0003212

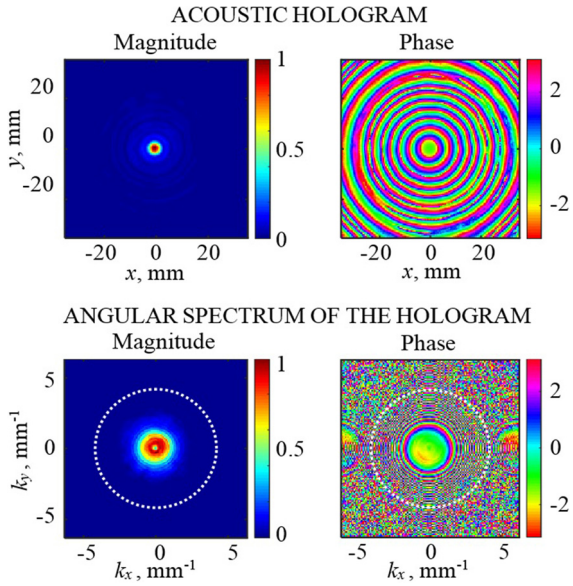

FIG. 5. (Color online) (Top) Transverse distribution of the magnitude and phase of the pressure field at a frequency of 1 MHz (acoustic hologram) measured at a distance $z_H = 73.5$ mm. (Bottom) Magnitude and phase of the corresponding angular spectrum. A circle (dotted curve) of radius $k = \omega/c_0$ indicates the boundary of the region of propagating plane waves.

5. Measurement of the propagator

The propagator, which carries information about the acoustic properties of a sample inserted between the transducer and the hydrophone, is determined from two-dimensional distributions of the complex amplitudes of the angular spectrum. These amplitudes are calculated from hydrophone measurements recorded in the free field and with the test sample in the propagation path [Eq. (12)]. As shown in Appendix A, the possible non-perpendicularity of the layer with respect to the axis z of the positioning system can be taken into account by shifting the origin of spatial frequencies to the extremum point of the propagator, $(k_x^{(n)}, k_y^{(n)})$. After this shift, it can be assumed that the measured propagator corresponds to the perpendicular arrangement of the layer and the corresponding equations from Sec. II A 2 can be applied.

To find the acoustic properties of the layer material, it is sufficient to use the propagator for only the spatial frequency that corresponds to normal incidence. The magnitude and phase of the propagator are then given by Eqs. (22) and (23), respectively, and the algorithm for finding the phase velocity and absorption coefficient is given by Eqs. (24) and (25). However, as previously mentioned, improved accuracy can be achieved by calculating the indicated parameters at other spatial frequencies in the vicinity of the normal incidence frequency and then averaging the results using Eqs. (27) and (28).

The relevant region of small spatial frequencies is shown in more detail in Fig. 6. This region is where the magnitude of the angular spectrum components from each measured hologram appreciably exceeds the noise level. If this region is chosen too wide so that the spectrum magnitude reaches the noise level, a noticeable error may occur when calculating the propagator expressed by the ratio of

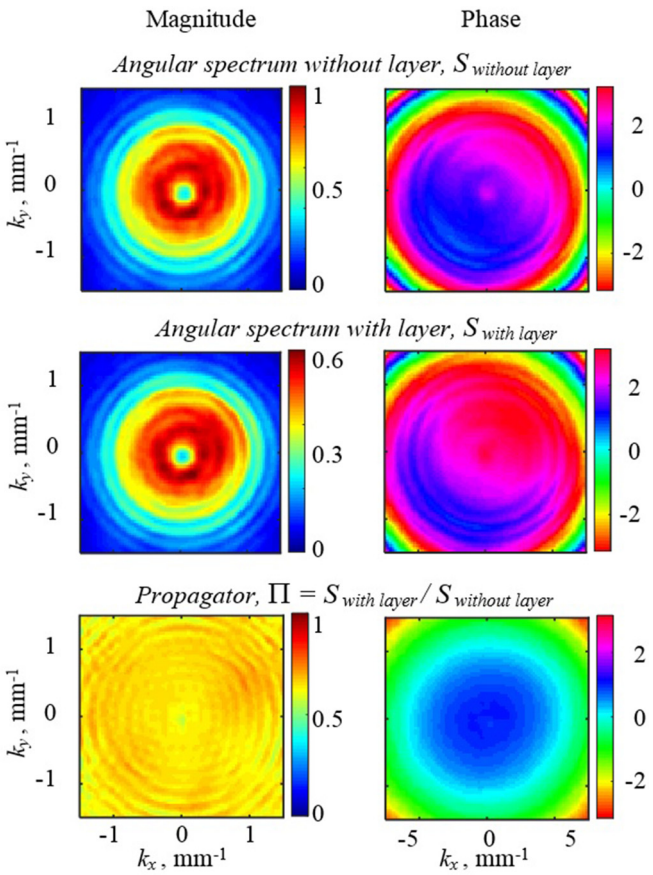

FIG. 6. (Color online) Reconstruction of a propagator at a frequency of 1 MHz from holograms measured at a distance $z_H = 73.5$ mm. The magnitude (on the left) and phase (on the right) of the angular spectrum are shown in the absence (top row) and presence (center row) of sample D20. The reconstructed propagator is shown at the bottom.

the spectra. Noisy regions that were excluded from propagator calculations appear blue in the two-dimensional distributions shown in Figs. 5 and 6.

When using a focused source with known diameter d and focal length F, the width of its angular spectrum can be estimated as the angle between the source axis and the ray directed from the edge of the source to the focal point, i.e., $k_{\max}/k_0 \approx d/(2F)$. Accordingly, a region on the plane (k_x, k_y) within a circle of radius $k_{\max}$ can be identified to contain sufficient information for making plane wave estimates of the phase velocity and absorption coefficient. For the source used in this study ($d = 38.1$ mm, $F = 63.5$ mm, $c_0 = 1.5$ mm/μs), $k_{\max}(\text{mm}^{-1}) \approx 1.26 \times f(\text{MHz})$. As can be seen from Fig. 6, this estimate for the frequency of 1 MHz is in good agreement with the measured results. The number of discrete spatial frequencies inside the indicated circle increases quadratically with frequency f and can be estimated as $620 \times (f(\text{MHz}))^2$. In the megahertz frequency range, this number of points is on the order of several hundred. Averaging over this large number of angular spectrum components allows for a significant improvement in the accuracy of absorption coefficient and phase velocity estimates. Typical standard deviations for the absorption coefficient and phase velocity measurements in the frequency

range from 0.4 to 1.6 MHz were $0.3\,\mathrm{m}^{-1}$ and 0.5 m/s, respectively.

When calculating the phase velocity from experimentally measured holograms, the propagator phase $\Phi_\Pi(k_x, k_y, \omega)$ is used, which is specified in an interval of length 2π, for example $[-\pi, \pi]$. Formal application of Eq. (12) for calculating the propagator $\Pi(k_x, k_y, \omega)$, therefore, yields not a total phase Φ_Π but a quantity $\varphi_\Pi \in [-\pi, \pi]$ that is related to the total phase by the expression $\Phi_\Pi(k_x, k_y, \omega) = \varphi_\Pi(k_x, k_y, \omega) + 2\pi N(k_x, k_y, \omega)$, where $N = N(k_x, k_y, \omega)$ is an integer that depends on frequencies (k_x, k_y, ω) and is not known in advance. Thus, before calculating the phase velocity, it is necessary to unwrap the phase by finding $N(k_x, k_y, \omega)$. The phase unwrapping procedure can be carried out based on the measured difference $\Delta t_{\mathrm{front}}$ in the arrival times of the pulses recorded by hydrophone on the beam axis as introduced by the presence of a test layer in the propagation path. This difference is equal to $\Delta t_{\mathrm{front}} = H(c_{\mathrm{front}}^{-1} - c_0^{-1})$, where c_{front} is the propagation speed of the pulse front. Since the dispersion of the phase velocity is small, $c(\omega) \approx c_{\mathrm{front}}$, the phase incursion for zero spatial frequency is $\Phi_\Pi(0, 0, \omega) \approx \omega\,\Delta t_{\mathrm{front}}$ as follows from Eq. (18). Taking into account that the calculated value for the phase difference $|\Phi_\Pi - \omega\,\Delta t_{\mathrm{front}}| < \pi$, the number of complete cycles N can be found as

$$N(0,0,\omega) = \mathrm{floor}\left(\frac{\omega\,\Delta t_{\mathrm{front}} - \varphi_\Pi(0,0,\omega)}{2\pi} + \frac{1}{2}\right), \qquad (34)$$

where the function floor$(\cdots)$ denotes the operation of extracting the integer part of a number. The total phase $\Phi_\Pi(0, 0, \omega)$ then can be determined and used as a starting value for the algorithm of phase unwrapping on the entire plane (k_x, k_y). Because the propagator phase front is a smooth surface, it can be assumed that there are no sharp phase jumps (by an amount greater than π) of the discrete spatial spectrum at neighboring points. Therefore, the phase unwrapping algorithm sequentially sorts all the points of a given region of spatial frequencies by moving from the current point (k_x, k_y) at which the phase is already found to its nearest neighbor $(\hat{k}_x, \hat{k}_y)$, where $\hat{k}_x = k_x \pm \Delta k$ or $\hat{k}_y = k_y \pm \Delta k$. In this case, the phase should be unwrapped in accordance with a formula similar to Eq. (34)

$$N\left(\hat{k}_x,\hat{k}_y,\omega\right) = \mathrm{floor}\left(\frac{\Phi_\Pi(k_x,k_y,\omega) - \varphi_\Pi\left(\hat{k}_x,\hat{k}_y,\omega\right)}{2\pi} + \frac{1}{2}\right). \qquad (35)$$

An arbitrary trajectory of the transition from point to point can be chosen; here, enumeration of points was done line by line, as in raster scanning.

B. Experimental results

1. Holographic reconstruction of the source surface vibration and acoustic beam structure

Although the main purpose of using the holographic method in this study was to analyze the propagation of plane waves, the holography-based reconstruction of the pattern of vibration of the source surface and the spatial structure of the radiated ultrasonic field were also of interest.[15,16] As already noted, the source was a single-element piezoelectric transducer with focusing provided by the concave shape of the radiating piezoelectric plate. For such transducers, the common oscillation pattern of their surface is uneven as a result of the peculiarities of the attachment of electrical contacts, the nature of the backing, as well as the inevitable excitation of Lamb waves in the piezoelectric plate.[21,22] Since the structure of the oscillations depends on the design features of the transducer, the influence of which on the vibration of the piezoelectric plate is difficult to model, an accurate theoretical prediction of the distribution of the vibrational velocity on the piezoelectric plate is usually impossible. The holography approach allows for reconstruction of the actual wave sources from the radiated field.

When performing holographic reconstruction of the transducer behavior, it is necessary to know the position of its surface in space. Since the piezoelectric plate had the shape of a spherical segment, it was sufficient to indicate the center of the corresponding sphere. To approximate the location of such a center, a point on the beam axis was determined at which the wave amplitude at the center frequency of 1 MHz reached a maximum ($z = 63.5$ mm). Note that due to diffraction, this point is located closer to the source than the true center of curvature of the radiating surface.[23] However, this difference for the transducer used here is fairly small and was neglected when defining the location of its center of curvature.

A nonstationary hologram was measured beyond the focus at a distance of 73.5 mm from the source. Based on these measurements, continuous wave holograms were found at different frequencies (one of them is shown in the top of Fig. 5) and used to backpropagate the field to the surface of the source using the Rayleigh integral.[15,16] To more evenly take into account the waves propagating from the source at large angles to the axis, the measured hologram was multiplied by a circular spatial window with a diameter of $D = 70$ mm, which suppressed the angular parts of the initial square hologram and thereby made it more adequate to the round shape of the source.

Figure 7 shows the results of reconstructing the magnitude and phase of the normal component of the vibrational velocity on the surface of the radiator at several characteristic frequencies. At all frequencies, the radiating region is a circle with a diameter of about 38 mm, which corresponds to the nominal size of the transducer. The inhomogeneous pattern of the surface vibrations is clearly visible in the form of a ring structure caused by quasi-standing Lamb waves. Despite slight differences in the reconstructed distributions, the surface of the radiator was completely active with no noticeable defects for all of the excitation frequencies.

The measured hologram also allowed reconstruction of the spatial structure of the acoustic field. Figure 8 shows the distribution of the acoustic pressure amplitude in the axial plane $(x = 0, y, z)$ calculated at the same frequencies

https://doi.org/10.1121/10.0003212

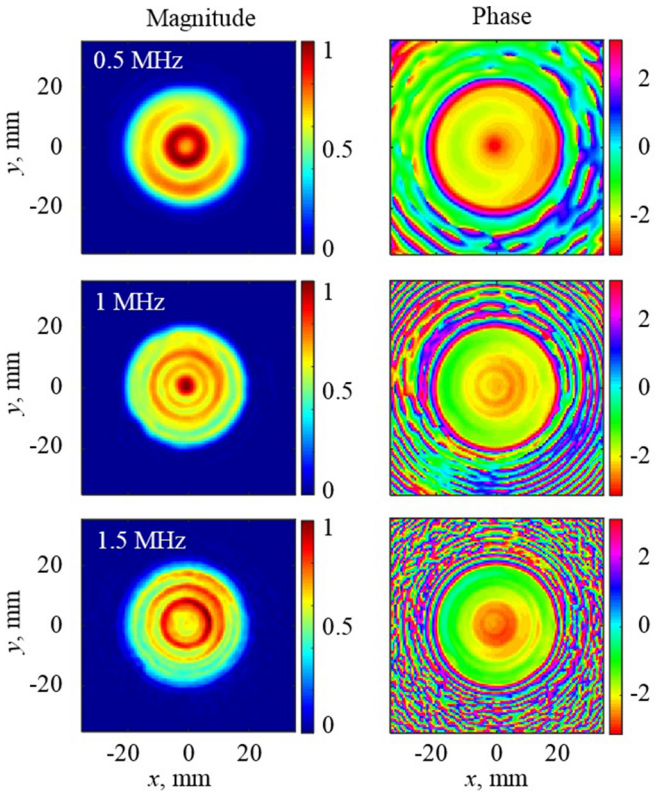

FIG. 7. (Color online) The magnitude (left column) and phase (right column) of the normal component of the vibrational velocity on the surface of the source at different excitation frequencies: 0.5 MHz (top), 1 MHz (center), and 1.5 MHz (bottom). The magnitude is normalized to its maximum value. The vibrational velocity was calculated based on the hologram measured at 73.5 mm from the source.

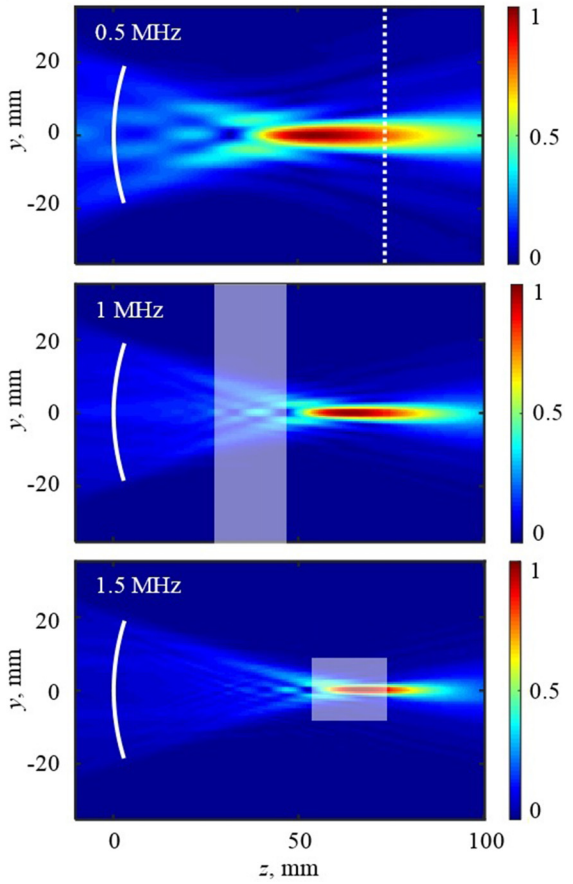

FIG. 8. (Color online) Distributions of the acoustic pressure amplitude in water in the absence of samples, reconstructed from the hologram in the axial plane of the beam at different frequencies, 0.5 MHz (top), 1 MHz (center), and 1.5 MHz (bottom). The amplitude is normalized to its maximum value. The white arc on the left indicates the surface of the source. The vertical dashed line in the top image depicts the measurement plane. The highlighted rectangular areas in the central and lower images indicate the position of the test samples (D20 and C20, respectively) during measurement.

as in Fig. 7. The white arc on the left corresponds to the radiating surface. The position of the scanning plane of the transverse distribution of the acoustic field parameters is depicted by a vertical dotted line in the upper image. The measured hologram was used to calculate both forward propagation (i.e., to the right relative to the plane of the hologram) and backward propagation to the source. The amplitude distribution to the left of the radiating surface was not physically realized and is shown only to demonstrate the backpropagation algorithm.

It can be seen from Fig. 8 that the ultrasonic field has the form of a focused beam and with increasing frequency, the degree of narrowing of the beam in the focus region increases. A theoretical calculation for the beam diameter determined from the minima of the wave amplitude closest to the axis for frequencies of 0.5, 1, and 1.5 MHz yields 12.2, 6.1, and 4.1 mm, respectively.[23] The corresponding values for the beams shown in Fig. 8 are 10.3, 6.1 and 4.2 mm, which are quite consistent with theoretical estimates.

Another feature of the field structure at different frequencies is the frequency-dependent diffraction shift toward the source of the point at which the maximum amplitude is reached (focal shift). Apparently, this effect was first noted in Ref. 23 where it was shown that for a uniformly oscillating radiator having the shape of a concave spherical cup with a depth h and radius of curvature F, the focal shift depends on the parameter k_0h as $\Delta z \approx 12F/[(k_0h)^2 + 12]$.

Given the geometric dimensions of the source used here, the theoretical shifts Δz at frequencies of 0.5, 1 and 1.5 MHz are approximately 15.4, 4.7, and 2.2 mm, respectively. It is interesting to compare the position of maximum amplitude at different frequencies with the position of the nominal focus of the radiator, which was defined as the point with maximum amplitude at an operating frequency of 1 MHz. From the above values of the shifts for an idealized source, it turns out that at a frequency of 0.5 MHz, the maximum amplitude point should shift toward the transducer by −9.7 mm and at a frequency of 1.5 MHz, on the contrary, it should move away by+2.5 mm. These focal shifts are close to the observed focal shifts, which for the distributions shown in Fig. 8 are −8.6 and +2.2 mm, respectively. The discrepancies can be explained by the uneven nature of the oscillations of the surface of the radiator (see Fig. 7).

For the phase velocity and absorption coefficient measurements, the samples were placed between the transducer

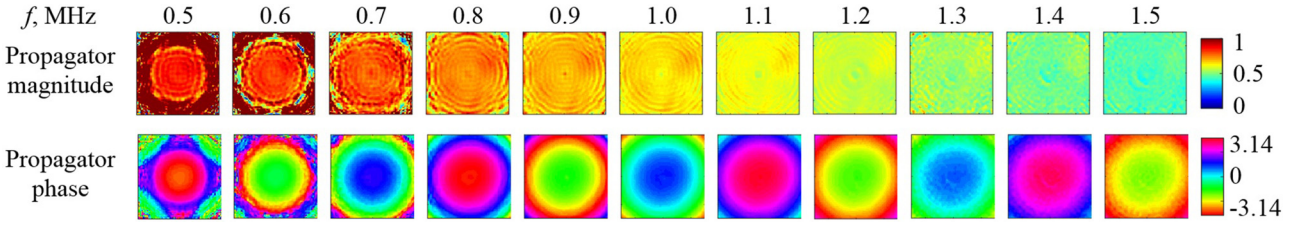

FIG. 9. (Color online) Distribution of the magnitude A_Π and phase Φ_Π of the propagator over a portion $|k_x|$, $|k_y| \le 1.5\,\mathrm{mm}^{-1}$ of the spatial frequency plane (k_x, k_y) at different frequencies $f = \omega/(2\pi)$ for the sample D20.

and the focus. In Fig. 8, bright rectangles schematically show the location of the samples against the background of the structure of acoustic beams with which the samples were measured. The center image shows the position of a large disk-shaped sample, and the bottom image shows a small cuboid-shaped one (see Fig. 1). Due to the transverse localization of the focused beam, both the disk-shaped sample and the smaller cuboid-shaped sample had transverse sizes noticeably larger than the beam diameter.

2. Propagator for layers of various thicknesses

As noted in Sec. III A 5, holograms of an acoustic beam, measured in the same plane in the presence of a layer and in its absence, make it possible to determine the propagator $\Pi(k_x, k_y, \omega)$. For the source used in this work, one could expect a high accuracy of the propagator measurements for spatial frequencies (k_x, k_y) inside the circle $k_x^2 + k_x^2 \le k_{\max}^2$ for which the estimate $k_{\max}(\mathrm{mm}^{-1}) \approx 1.26 \times f(\mathrm{MHz})$ is valid. The indicated feature is visible in Fig. 9 in which the results of measuring the propagator at various frequencies are shown for sample D20. The magnitude A_Π and phase Φ_Π distributions on the plane (k_x, k_y) are shown within the square $|k_x|, |k_y| \le 1.5\ \mathrm{mm}^{-1}$. The propagator magnitude distributions show, especially at low frequencies of 0.5, 0.6, and 0.7 MHz, that near the origin there is a region of relatively uniform color in the form of a circle whose radius increases with frequency. The indicated circle corresponds to the area where the propagator measurement is little affected by noise. With increasing frequency, the propagator magnitude decreases, which is due to a corresponding increase in the absorption coefficient. The propagator phase distribution also depends on the frequency, while the color picture has an axially symmetric shape with the center at the origin, which confirms the high degree of parallelism of the sample and the field scanning plane.

As noted above, the propagator values $\Pi(k_x, k_y, \omega)$ over a large number of spatial frequencies allow statistical averaging and refinement of the sound velocity and absorption coefficient. If we average over k_x, k_y in Eqs. (17) and (18) to generate initial estimates for $c(\omega)$ and $\alpha(\omega)$, then these values can be substituted into Eqs. (22) and (23) to obtain a more accurate estimate for the propagator $\Pi(0, 0, \omega)$. Figure 10 shows the corresponding frequency dependences of the propagator magnitude A_Π (upper plots) and propagator phases Φ_Π (central plots) for various samples.

It can be seen that in the frequency range from 0.4 to 1.6 MHz, the propagator magnitude decreases monotonically, which indicates an increasing character of the frequency dependence of the absorption coefficient. For thicker specimens, the decay is faster. The propagator phase is shown after the unwrapping operation described in Sec. III A 5. The phase value Φ_Π grows almost linearly with frequency, which reflects the small dispersion of the phase velocity.

The bottom part of Fig. 10 shows the results of the calculation of the filtered impulse response $g(t)$ expressed by Eq. (26) but with integration only at the interval $0.4\ \mathrm{MHz} \le |\omega|/(2\pi) \le 1.6\ \mathrm{MHz}$, where the noise level is small. As expected, the impulse response takes the form of a short pulse, which experiences a delay that increases with increasing sample thickness. In addition, faster absorption of high frequencies leads to the fact that with an increase in the sample thickness, the peak value of the impulse response decreases and the duration increases.

3. Absorption coefficient and phase velocity

The main purpose of the proposed method for extracting plane waves from the experimental holograms was to

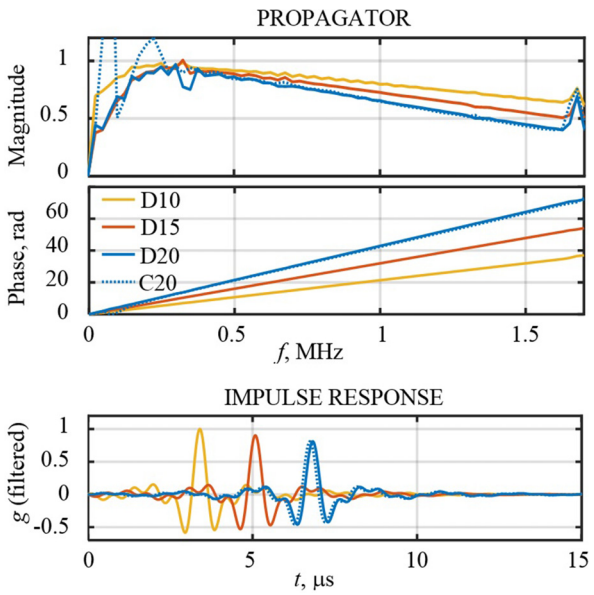

FIG. 10. (Color online) The frequency dependence of the magnitude A_Π (top) and phase Φ_Π (center) of the propagator for different samples. The correspondence of the color of the curves to the samples is explained in the central graph. (Bottom) Impulse response calculated by integration over the frequency range from 0.4 to 1.6 MHz.

https://doi.org/10.1121/10.0003212

measure the absorption coefficient and phase velocity of the acoustic waves. The results of these measurements are shown in Fig. 11. The values of the acoustic parameters of the material given in Fig. 11 were obtained by averaging the values of $1/c^{(k_x,k_y)}$ and $\alpha^{(k_x,k_y)}$, represented by Eqs. (27) and (28), respectively, over the components of the angular spectrum within a circle of radius $k_{\max}(\mathrm{mm}^{-1}) \approx 1.26 \times f(\mathrm{MHz})$. The top graph shows the frequency dependences of the absorption coefficient found for all four samples using the propagator. In addition, a curve calculated based on measurements of total acoustic power using Eq. (31) was added for sample D20.

The bottom graph in Fig. 11 shows the frequency dependences for the shift of the phase velocity relative to its value at the frequency $f_1 = 1$ MHz: $\Delta c = c(f) - c(f_1)$. The calculated phase velocity values $c(f_1)$ for different samples were 980.6, 983.8, 982.5, and 986.7 m/s for samples D10, D15, D20, and C20, respectively. The indicated discrepancy can be explained by the limited accuracy of specifying the thickness of the samples (see Table I), which is used to calculate the phase velocity value based on the measured propagator phase. As can be seen, the estimate 983.4 ± 3 m/s is valid for speed $c(f_1)$. It is useful to compare this value with the wavefront propagation velocity, measured based on the shift of the delay times of the arrival of the signal front with and without a layer. The indicated shifts for samples D10, D15, D20, and C20 were 3.37, 5.13, 6.85, and 6.82 μs, which gives velocities of 984, 981, 982, and 983 m/s, respectively, i.e., the measured velocity of the signal front was 982.5 ± 1.5 m/s. As can be seen, this value is close to the obtained results for the velocity $c(f_1)$.

IV. DISCUSSION

A. Absorption coefficient

The results for the frequency dependence of the absorption coefficient shown in Fig. 11 indicate a high repeatability of the measurement results when using samples of different thicknesses. It can be seen that within the frequency range from 0.4 to 1.6 MHz, which contains most of the energy of the acoustic signal, the curves for samples D10, D15, and D20 are practically indistinguishable.

A significant result illustrating the operability of the coefficient measurement method proposed in this work is the coincidence of the absorption curves for the sample D20, which is extended in the transverse direction, and the sample C20, which is small in size but has the same thickness. Thus, due to the use of a beam localized in the transverse direction, it was possible to measure the absorption coefficient, which characterizes the behavior of an infinite plane wave, using a small sample.

To analyze the proximity of the experimental curves $\alpha(f)$ to each other, the deviation of these curves from a certain averaged or fitted curve $\bar{\alpha}(f)$ was considered. The fitted curve was constructed from the experimental data for the thickest sample D20 in the frequency range from 0.4 to 1.6 MHz, where the measurement errors were minimal and, thus, was assumed to be close to the true dependence. An analysis showed that the experimental data are described with high accuracy by the following power law:

$$\bar{\alpha}(f) = \alpha_1 (f/f_1)^{\eta}, \tag{36}$$

where $f_1 = 1$ MHz, $\alpha_1 = 21.17\ \mathrm{m}^{-1}$ is the absorption coefficient at the frequency f_1, and $\eta = 1.585$ is an exponent. The upper part of Fig. 12 shows plots for the frequency dependence of the relative deviation $\delta\alpha = (\alpha - \bar{\alpha})/\bar{\alpha}$, expressed as a percentage, for various samples. The lower part of Fig. 12 shows the spectra of two signals normalized to their maximum value: the hydrophone signal already shown earlier in Fig. 4 (solid line) and the voltage signal supplied to the transducer (dashed line). These frequency dependences indicate that within the frequency range from 0.4 to 1.6 MHz, where the spectral amplitude of the acoustic signal

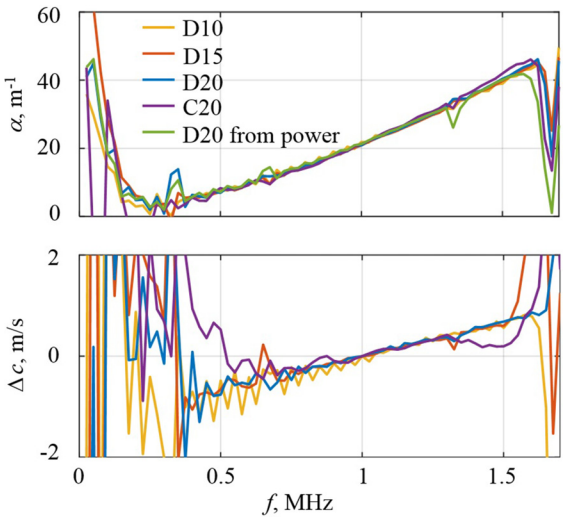

FIG. 11. (Color online) The frequency dependences of the absorption coefficient (top) and phase velocity (bottom) for various samples using averaging over a circle of radius $k_{\max}(\mathrm{mm}^{-1}) \approx 1.26 \times f(\mathrm{MHz})$.

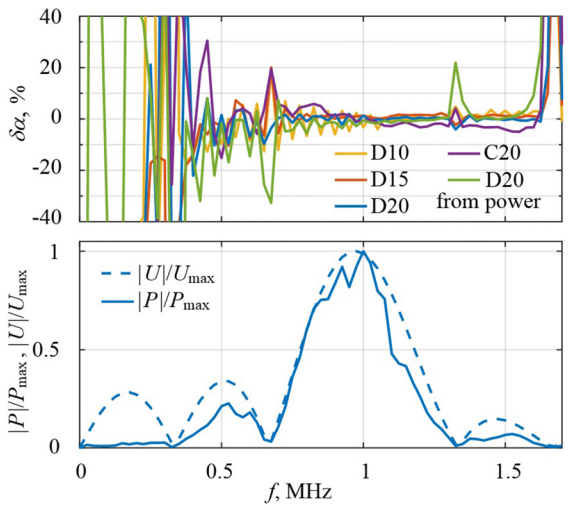

FIG. 12. (Color online) (Top) The frequency dependence of the relative deviation of the absorption coefficient from Eq. (36). (Bottom) The spectral amplitude of the signals applied to the transducer and recorded by the hydrophone, normalized to their maximum values.

is not too small, the spread in the results of measuring the absorption coefficient does not exceed 5%–10%. An exception is the vicinity of frequencies of 0.7 and 1.35 MHz, where the spectral amplitude of the electric signal at the source and, as a consequence, the amplitude of the acoustic signal at the hydrophone have local minima. Thus, as expected, the error in measuring the absorption coefficient is large at those frequencies where the amplitude of the acoustic signal is small. Within the frequency band, where the signal significantly exceeds the noise level, the spread of the absorption curves is small, which indicates the high accuracy and good repeatability of the proposed method for measuring the absorption coefficient.

Figures 11 and 12 show not only curves derived from estimates for the absorption coefficient based on measurements of the propagator but also a curve for sample D20 obtained by measuring the total acoustic power. The corresponding dependence for the absorption coefficient appeared to be very close to the dependences determined from the propagator measurement. As noted in Sec. II A 4, the method based on measuring acoustic power is more accurate when the angular spectrum of the probe beam is narrower. Despite the approximate nature of this method, it has one important advantage, namely, that its use does not require strict plane parallelism and uniformity of the test sample. This advantage may turn out to be fundamental in characterizing media that by their nature have a certain heterogeneity, for example, biological tissues.

B. Phase velocity

As can be seen from the bottom graphs in Fig. 11, the results for the frequency-dependent shift of the phase velocity $\Delta c = c(f) - c(f_1)$ vary slightly for different samples in the operating frequency range from 0.4 to 1.6 MHz, especially for the disk-shaped samples D10, D15, and D20. There is some larger difference at low frequencies for the small cuboid sample C20, which may be due to the fact that the side lobes of the probe beam partially do not fall on the sample, which causes distortion of the propagator phase.

As already noted, the calculated values of the phase velocity at the frequency $f_1 = 1$ MHz for different samples were slightly different: $c(f_1) = 983.4 \pm 3$ m/s. This difference can be explained by the limited accuracy of measuring the thickness of the samples. According to Table I, the relative error in the thickness measurement ranged from 0.25% to 0.5%, which, in accordance with Eq. (24), yields the same (apparent) relative error in the value of the phase velocity. In absolute units, this error is from 2.5 to 5 m/s, which corresponds to the marked spread for the phase velocity $c(f_1)$. Note that a different source of systematic measurement error could be the temperature inconsistency during the measurement of holograms for different samples. The temperature coefficients of the speed of sound dc/dT for water and RTV are 2.75 ± 0.01 and -2.8 ± 0.1 (m/s)/K, respectively.[24,25] Estimates based on these values show that the resulting velocity spread could be observed with temperature changes of more than half a degree. During the experiments, such fluctuations were not observed; therefore, it can be assumed that the main reason for the apparent difference in the phase velocity in various samples was the errors in measuring thicknesses.

A characteristic feature of the experimental frequency dependences of the phase velocity shown in Fig. 11 is their growth with frequency. According to the causality principle, the dispersion of the phase velocity is interconnected with the frequency dependence of the absorption coefficient. From this point of view, the results obtained are useful to analyze in more detail. Figure 13 shows the dependences obtained from the measured propagator for the absorption coefficient and phase velocity for sample D20. In contrast to Fig. 11, the experimental results are depicted not by curves but by individual experimental points representing the values of the quantities at the corresponding frequencies of the discrete Fourier transform. The solid curve in the top of Fig. 13 corresponds to the power law dependence [Eq. (36)]. It can be seen that the experimental points accurately fit the indicated power dependence within the frequency range from 0.4 to 1.6 MHz. Given the smooth behavior of the dispersion curves, the integral dispersion relations can be replaced by approximate local relations.[26] It was shown that, in the case of a power law dependence of the absorption coefficient $\alpha = \alpha_1 (f/f_1)^\eta$ with $0 \le \eta \le 2$, local dispersion relations allow the phase velocity to be expressed with high accuracy using the following equation:[27]

$$c(f) = \frac{c(f_1)}{1 + \dfrac{\alpha(f_1)c(f_1)}{2\pi f_1} \tan\left(\dfrac{\pi}{2}\eta\right)\left[\left(\dfrac{f}{f_1}\right)^{\eta-1} - 1\right]}. \quad (37)$$

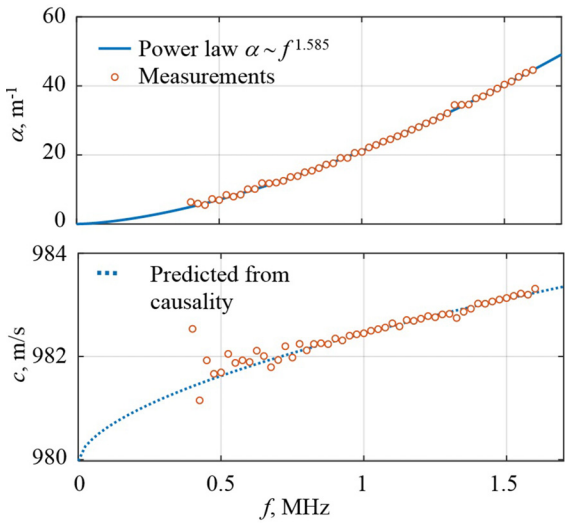

FIG. 13. (Color online) Dispersion dependences for sample D20. (Top) The absorption coefficient. (Bottom) The phase velocity. The circles show the experimental values obtained based on the measured propagator. The smooth curve in the upper graph corresponds to a power approximation $\alpha \sim f^\eta$. The dashed curve in the lower graph is constructed using the indicated dependence based on local dispersion relations.

https://doi.org/10.1121/10.0003212

In the bottom graph in Fig. 13, the dashed curve is constructed from Eq. (37) using the power law parameters drawn by a solid curve in the upper graph. We note very good agreement between the experimental results and the dependence predicted from the causality principle.

C. Impact of the hydrophone size on propagator measurement

The propagator-based method presented in this study relies on the measurement of acoustic holograms. In general, the correct measurement of a hologram requires the use of a miniature hydrophone that has a sensitive element with a diameter less than a wavelength (preferably much less).[16] The sensitivity of such hydrophones is low, limiting their capability of detecting weak signals against a background of noise, which is especially noticeable when conducting broadband measurements using short pulses.

A hydrophone is much more sensitive if its diameter is comparable to the wavelength or exceeds it. The obvious drawback of larger receivers, however, is the fact that they do not show the true signal at a point, but they show the result of the acoustic pressure averaged over the surface of the sensitive region.[28,29] The corresponding effect of spatial non-locality is equivalent to the fact that the sensitivity of a finite-size hydrophone is direction dependent. In terms of the angular spectrum, the corresponding radiation pattern can be described using some frequency-dependent function for the directivity $D(k_x, k_y, \omega)$. In turn, the sensitivity of the hydrophone at normal incidence to a plane wave (when $k_x = k_y = 0$) should be scaled in order to account for the sensitivity to each obliquely incident plane wave in the angular spectrum. Thus, when using a hydrophone of a finite size, a quantity $D(k_x, k_y, \omega) \times S(k_x, k_y, z, \omega)$ is measured instead of the true angular spectrum $S(k_x, k_y, z, \omega)$.

However, the propagator is defined as the ratio of angular spectra such that the factor $D(k_x, k_y, \omega)$ present in both the denominator and the numerator is canceled—see Eq. (12). In other words, the use of a finite-size hydrophone does not introduce any error into the propagator measurement. Of course, this conclusion is valid only for those spatial frequencies where the value $|D(k_x, k_y, \omega)|$ is not too small compared to unity so that the amplitude of the corrected angular spectrum noticeably exceeds the noise level.

For example, consider the sensitive section of the hydrophone to be a circle of radius a. To assess the directivity in this case, one can use the recommendation of the International Electrotechnical Commission (IEC 62127–3, section 5.6), according to which for a circular receiver inserted in a rigid baffle, the directivity diagram has the form $2J_1(k_0 a \sin\theta)/(k_0 a \sin\theta)$, where $J_1(\cdot)$ is the Bessel function, $k_0 = \omega/c_0$ is the wavenumber, and θ is the angle between the normal to the surface of the hydrophone and the direction of propagation of the received wave.[30,31] It follows that

$$D(k_x, k_y, \omega) = \frac{2\,J_1\left(\sqrt{k_x^2 + k_y^2}\,a\right)}{\sqrt{k_x^2 + k_y^2}\,a}. \tag{38}$$

The area on the spatial frequency plane, where the directivity function $D(k_x, k_y, \omega)$ exceeds a given level, is a circle $\sqrt{k_x^2 + k_y^2} \le k_a$. The radius of this circle at the level $|D| = 0.1$, according to Eq. (38), is equal to $k_a \approx 3.42/a$. It is interesting to compare this radius with the radius of the circle $k_{\max}(\mathrm{mm}^{-1}) \approx 1.26 \times f(\mathrm{MHz})$ that was previously used when averaging the propagator over spatial frequencies. The final size of the hydrophone will not affect the measurement results at $k_a > k_{\max}$, whence the following estimate is obtained for the permissible radius of the hydrophone: $a(\mathrm{mm}) < 2.71/f(\mathrm{MHz})$. For example, for a frequency of 1 MHz, the diameter of the hydrophone can reach 5.4 mm, which is much larger than the diameter of the hydrophone used in the experiments (0.4 mm) and more than three times the wavelength. Thus, the proposed method for measuring the propagator can be implemented using even larger and, therefore, more sensitive receivers. Note that with an increase in the diameter of the hydrophone, its directivity becomes narrower, which results in low-pass filtering of the angular spectrum. According to the Nyquist criterion, this allows for increasing the scanning step and, thus, faster measurement of the propagator without significant loss of accuracy. However, if noticeable side lobes are present in the directivity, the scanning step should be kept small (half the wavelength or less) in order to avoid aliasing effects.

D. Conclusions

In this study, a method is described for measuring the acoustic characteristics of media based on the possibility of using bounded acoustic beams and finite-size samples to analyze the behavior of unbounded plane waves passing through a test sample of finite thickness and infinite lateral dimensions. The proposed method is based on the theoretical decomposition of the acoustic field into an angular spectrum to describe a wave beam as a superposition of plane waves traveling in different directions. Experimentally, the method relies on nonstationary acoustic holography measurements, i.e., measurement of acoustic waveforms over a distribution of points on some surface that intersects the beam. Harmonic plane waves of different directions, selected using the hologram as a result of spectral decompositions in time and transverse coordinates, allow for the measurement of the acoustic characteristics of materials within a certain frequency range. It was shown that the accuracy of measurements at a given frequency can be improved by using a large number (up to several hundred or more) of plane waves probing the test layer at different angles. One of the important advantages of the proposed method is the ability to accurately measure the absorption coefficient and phase velocity in the near field of acoustic sources when

using small samples. It should be also noted that in traditional approaches, the effects of near-field diffraction and refraction at the sides of the layer can affect the accuracy of measuring the absorption coefficient. Corresponding errors are reduced by placing the hydrophone in the far field of the source. In this case, the correction for diffraction and refraction can be made on the assumption of spherical divergence of the wave.[6] However, this approach becomes more difficult at high frequencies when a greater distance between the source and receiver is required. The proposed method allows measurements in the near field and naturally takes into account the effects of diffraction and refraction.

ACKNOWLEDGMENTS

This work was supported in part by the Russian Science Foundation (RSF) under Grant No. 19-12-00148 and, in part, by the National Institutes of Health (NIH) under Grant No. R01-EB025187.

APPENDIX A: BEAM TRANSMISSION THROUGH AN INCLINED LAYER

It is assumed that the axis of the acoustic beam is directed close to the z axis of the positioner that is used to measure the hologram. However, the orientation of a test layer may not be exactly perpendicular to the axis z. We will call this position *inclined*. Let $\mathbf{n} = (n_x, n_y, n_z)$ be the unit normal to the layer surface. In the case when the layer is perpendicular to the positioner axis z, $\mathbf{n} = (0, 0, 1)$. Consider the passage of angular spectrum components through a test layer, which in a liquid has the form of a plane wave $e^{i\mathbf{k}_0\cdot\mathbf{r}}$ with a wave vector $\mathbf{k}_0 = (k_x, k_y, k_z = \sqrt{k_0^2 - k_x^2 - k_y^2})$ so that $|\mathbf{k}_0| = k_0$. We represent this wave vector in the form $\mathbf{k}_0 = \mathbf{k}_\perp + \mathbf{k}_\parallel^{(0)}$, where $\mathbf{k}_\parallel^{(0)} = k_\parallel^{(0)}\mathbf{n}$ is the component directed along the normal, and $\mathbf{k}_\perp$ is the tangent to the surface of the component layer. After penetrating the layer, the wave takes the form $e^{i\mathbf{k}\cdot\mathbf{r}}$, where $|\mathbf{k}| = k$, $\mathbf{k} = \mathbf{k}_\perp + \mathbf{k}_\parallel$, and $\mathbf{k} = k\mathbf{n}$. Due to the boundary condition, the tangent component of the refracted wave vector is the same as the incident wave vector, whereas its normal component is generally different. We rewrite the previously obtained Eq. (12) using the notation introduced as

$$\Pi(k_x, k_y, \omega) = T_{\text{in-out}}\, e^{i\left(k_\parallel - k_\parallel^{(0)}\right)H}, \tag{A1}$$

where the transmission coefficient through two interfaces, $T_{\text{in-out}}$, is expressed by Eq. (13) in which normal impedances, according to Eqs. (14) and (15), respectively, can be written as $Z_0 = \rho_0\omega/k_\parallel^{(0)}$ and $Z = \rho\omega/k_\parallel$. Therefore, $T_{\text{in-out}}$ is expressed through $k_\parallel^{(0)}$ and $k_\parallel$. Now the propagator, according to Eq. (A1), is completely determined by the quantities $k_\parallel^{(0)}$ and $k_\parallel$, which can be written as

$$k_\parallel^{(0)}(k_x, k_y, \omega) = \mathbf{n}\cdot\mathbf{k}_0 = n_x k_x + n_y k_y + n_z\sqrt{k_0^2 - k_x^2 - k_y^2}, \tag{A2}$$

$$k_\parallel(k_x, k_y, \omega) = \sqrt{\mathbf{k}^2 - \mathbf{k}_\perp^2} = \sqrt{k^2 - k_0^2 + k_\parallel^{(0)2}}. \tag{A3}$$

These expressions generalize the definition of the propagator $\Pi(k_x, k_y, \omega)$ to the case of an inclined orientation of the test layer relative to the incident beam.

For a layer inclined at a slight angle, it is useful to consider the form of the propagator at the position in the angular spectrum that corresponds to the normal incidence. This location can be expressed as $(k_x^{(n)}, k_y^{(n)}) = k_0(n_x, n_y)$. Introducing the shifts $\tilde{k}_x = k_x - k_x^{(n)}$ and $\tilde{k}_y = k_y - k_y^{(n)}$, let us consider the case of small shifts $|\tilde{k}_x/k_0|, |\tilde{k}_y/k_0| \ll 1$. In the second order of smallness, the above definitions yield the following expression for the tangential component of the wave vector $\mathbf{k}_\perp$:

$$\mathbf{k}_\perp^2 \approx \tilde{k}_x^2 + \tilde{k}_y^2 + \left(n_x\tilde{k}_x + n_y\tilde{k}_y\right)^2/n_z^2. \tag{A4}$$

If we further consider that the slope is also small, i.e., $|n_x|, |n_y| \ll 1$, the last term in the right-hand side of Eq. (A4) can be omitted, which provides $\mathbf{k}_\perp^2 \approx \tilde{k}_x^2 + \tilde{k}_y^2$, i.e., the quantity $\mathbf{k}_\perp^2$ for a slightly inclined layer is expressed by the same formulas as in the case of the perpendicular arrangement with the only difference being that the spatial frequencies are shifted. Given that, now

$$k_\parallel^{(0)} = \sqrt{k_0^2 - \tilde{k}_x^2 - \tilde{k}_y^2} \tag{A5}$$

and

$$k_\parallel = \sqrt{k^2 - \tilde{k}_x^2 - \tilde{k}_y^2}, \tag{A6}$$

it follows that in terms of the shifted spatial frequencies $\tilde{k}_x$ and $\tilde{k}_y$, the propagator for a slightly inclined layer (which, as shown above, depends entirely on $k_\parallel^{(0)}$ and $k_\parallel$) is expressed by the same formulas as in the case of a perpendicular arrangement.

Note that because the magnitude $\mathbf{k}_\perp^2 = \tilde{k}_x^2 + \tilde{k}_y^2$ is zero during normal incidence, according to Eqs. (17)–(21) at the corresponding spatial frequencies $(k_x^{(n)}, k_y^{(n)})$, the propagator magnitude $A_\Pi(k_x, k_y, \omega)$ reaches its maximum, and the propagator phase $\Phi_\Pi(k_x, k_y, \omega)$ reaches a minimum or maximum (depending on the ratio of the speeds of sound in the layer and the immersion medium). Accordingly, the frequencies $(k_x^{(n)}, k_y^{(n)})$ can be readily identified in experimental data from the two-dimensional distributions of the propagator magnitude and phase at each frequency ω within the measured bandwidth.

APPENDIX B: CALCULATION OF DISCRETE FOURIER TRANSFORMS

The spectral transform, Eq. (3), takes the form of a discrete Fourier transform

https://doi.org/10.1121/10.0003212

$$P^{(m)}(\mathbf{r}) = h_t e^{im(2\pi/T)t_0} \sum_{n=0}^{N-1} p^{(n)}(\mathbf{r}) e^{i2\pi mn/N}. \quad \text{(B1)}$$

Here, h_t is the time discretization step, $T = Nh_t$ is the length of the time window, N is the number of sampling points, t_0 is the point in time corresponding to the beginning of the time window. The original time signal and its spectrum are associated with the corresponding discrete representations as follows: $p(\mathbf{r}, t_n) = p^{(n)}(\mathbf{r})$ for $t_n = t_0 + nh_t$, where $n = 0, 1, \ldots, N-1$, $P(\mathbf{r}, \omega_m) = P^{(m)}(\mathbf{r})$ for $\omega_m \geq 0$, $P(\mathbf{r}, \omega_m) = P^{(m+N)}(\mathbf{r})$ for $\omega_m < 0$, where $\omega_m = m\Delta\omega$, $m = -N/2, \ldots, 0, \ldots, N/2 - 1$, and

$$\Delta\omega = 2\pi/T \quad \text{(B2)}$$

is the sampling step on the cyclic frequency corresponding to the periodization of the signal with a period T. The discrete transform calculation, Eq. (B1), was performed using the fast Fourier transform (FFT) algorithm.

Similar to the time sampling procedure described above with respect to a signal at a given point, when scanning a field with a hydrophone, the signal is also sampled by transverse spatial variables. Consider in the plane of the hologram $z = z_H$, a square scan region of size $D \times D$ such that $-D/2 \leq x \leq D/2$ and $-D/2 \leq y \leq D/2$ (Fig. 2). The coordinates of the points at which the signal is measured by the hydrophone are recorded in the following form: $x = l_x h$, $l_x = -L/2, \ldots, 0, 1, \ldots, L/2 - 1$, $y = l_y h$, $l_y = -L/2, \ldots, 0, 1, \ldots, L/2 - 1$, where L is the number of sampling points along each direction, and h is the sampling step, i.e., $D = L\,h$. The corresponding discrete values

$$P(\mathbf{r}, \omega_m) = P(l_x h,\, l_y h,\, z_H, \omega_m) = P^{(m)}_{l_x l_y} \quad \text{(B3)}$$

allow one to write a discrete analog of Eq. (6):

$$S^{(m)}_{j_x j_y} = h^2 \sum_{l_x=-L/2}^{L/2-1} \sum_{l_y=-L/2}^{L/2-1} P^{(m)}_{l_x l_y} e^{-i(2\pi/L)(j_x l_x + j_y l_y)}, \quad \text{(B4)}$$

where $j_x = -L/2, \ldots, 0, 1, \ldots, L/2 - 1$, $j_y = -L/2, \ldots, 0, 1, \ldots, L/2 - 1$. The quantities $S^{(m)}_{j_x j_y}$ specify the initial angular spectrum in a discrete set of frequencies,

$$S\left(k_x = j_x \Delta k, k_y = j_y \Delta k, z_H, \omega = m\Delta\omega\right) = S^{(m)}_{j_x j_y}, \quad \text{(B5)}$$

where

$$\Delta k = 2\pi/D \quad \text{(B6)}$$

is the sampling step for spatial frequencies. As in the case of the time discretization described previously, the formulas written above represent the classical discrete Fourier transform. Due to the periodicity of the discrete spectra, $P^{(m)}_{l_x - L, l_y} = P^{(m)}_{l_x, l_y - L} = P^{(m)}_{l_x, l_y}$; therefore, summation in both sums in Eq. (B4) can be carried out from 0 to $L - 1$, i.e., it is possible to use the more familiar form of the discrete Fourier transform.

In order to avoid clipping of the useful signal and the effect of aliasing, the size of the spatial window was chosen to exceed the diameter of the ultrasonic beam and was equal to $D = 70$ mm, and the step of shifting the hydrophone when recording the hologram was $h = 0.5$ mm. The number of spatial steps in each of the transverse directions was $L = 140$.

[1]H. J. McSkimin, "Ultrasonic methods of measuring the mechanical properties of liquids and solids," *Physical Acoustics: Principles and Methods*, edited by W. P. Mason (Academic, New York, 1964), Vol. I, part A, Chap. 10, pp. 271–334.

[2]J. C. Bamber, "Attenuation and absorption," *Physical Principles of Medical Ultrasonics*, 2nd ed. (Wiley, New York, 2003), Chap. 4, pp. 93–166.

[3]J. C. Bamber, "Speed of sound," in *Physical Principles of Medical Ultrasonics*, 2nd ed. (Wiley, New York, 2003), Chap. 5, pp. 167–190.

[4]E. L. Madsen, F. Dong, G. R. Frank, B. S. Garra, K. A. Wear, T. Wilson, J. A. Zagzebski, H. L. Miller, K. K. Shung, S. H. Wang, and E. J. Feleppa, "Interlaboratory comparison of ultrasonic backscatter, attenuation, and speed measurements," J. Ultrasound Med. **18**(9), 615–631 (1999).

[5]F. W. Kremkau, R. W. Barnes, and C. P. McGraw, "Ultrasonic attenuation and propagation speed in normal human brain," J. Acoust. Soc. Am. **70**(1), 29–38 (1981).

[6]B. Zeqiri, W. Scholl, and S. P. Robinson, "Measurement and testing of the acoustic properties of materials: A review," Metrologia **47**(2), S156–S171 (2010).

[7]R. Bass, "Diffraction effects in the ultrasonic field of a piston source," J. Acoust. Soc. Am **30**(7), 602–605 (1958).

[8]V. A. Krasil'nikov and V. V. Krylov, *Introduction to Physical Acoustics* (Nauka, Moscow, 1984), in Russian.

[9]J. W. Goodman, *Introduction to Fourier Optics* (McGraw-Hill, New York, 1968).

[10]L. M. Brekhovskikh, *Waves in Layered Media*, 2nd ed. (Academic, New York, 1980).

[11]O. A. Sapozhnikov, "High-intensity ultrasonic waves in fluids: Nonlinear propagation and effects," in *Power Ultrasonics. Applications of High-Intensity Ultrasound* (Elsevier, Cambridge, 2015), Chap. 2, pp. 9–35.

[12]K. G. Krishnan, "Dispersion of ultrasonic velocity in liquids," Proc. - Indian Acad. Sci., Sect. A **9**(5), 382–385 (1939).

[13]J. M. M. Pinkerton, "A pulse method for the measurement of ultrasonic absorption in liquids: Results for water," Nature **160**(4056), 128–129 (1947).

[14]O. A. Sapozhnikov and M. R. Bailey, "Radiation force of an arbitrary acoustic beam on an elastic sphere in a fluid," J. Acoust. Soc. Am. **133**(2), 661–676 (2013).

[15]O. A. Sapozhnikov, Y. A. Pishchalnikov, and A. V. Morozov, "Reconstruction of the normal velocity distribution on the surface of an ultrasonic transducer from the acoustic pressure measured on a reference surface," Acoust. Phys. **49**(3), 354–360 (2003).

[16]O. A. Sapozhnikov, S. A. Tsysar, V. A. Khokhlova, and W. Kreider, "Acoustic holography as a metrological tool for characterizing medical ultrasound sources and fields," J. Acoust. Soc. Am. **138**(3), 1515–1532 (2015).

[17]L. E. Maggi, M. A. Von Krüger, W. C. A. Pereira, and E. E. C. Monteiro, "Development of silicon-based materials for ultrasound biological phantoms," in *Proc. 2009 IEEE Int. Ultrason. Symp.*, pp. 1962–1965 (2009).

[18]I. S. Grigoriev and E. Z. Meilikhov (eds.), *Handbook of Physical Properties* (CRC Press, New York, 1997).

[19]O. A. Sapozhnikov, A. E. Ponomarev, and M. A. Smagin, "Transient acoustic holography for reconstructing the particle velocity of the surface of an acoustic transducer," Acoust. Phys. **52**(3), 324–330 (2006).

[20]D. Nikolaev, S. Tsysar, A. Krendeleva, O. Sapozhnikov, and V. Khokhlova, "Using acoustic holography to characterize absorbing layers," Proc. Mtgs. Acoust. **38**, 045012 (2019).

[21]D. Cathignol, O. A. Sapozhnikov, and J. Zhang, "Lamb waves in piezoelectric focused radiator as a reason for discrepancy between O'Neil formula and experiment," J. Acoust. Soc. Am. **101**(3), 1286–1297 (1997).

[22]O. A. Sapozhnikov and M. A. Smagin, "Finding the dispersion relations for Lamb-type waves in a concave piezoelectric plate by optical visualization of the ultrasound field radiated into a fluid," Acoust. Phys. **61**(2), 181–187 (2015).
[23]H. T. O'Neil, "Theory of focusing radiators," J. Acoust. Soc. Am. **21**(5), 516–526 (1949).
[24]V. A. Del Grosso and C. W. Mader, "Speed of sound in pure water," J. Acoust. Soc. Am. **52**(5B), 1442–1446 (1972).
[25]D. L. Folds, "Speed of sound and transmission loss in silicone rubbers at ultrasonic frequencies," J. Acoust. Soc. Am. **56**(4), 1295–1296 (1974).
[26]M. O'Donnell, E. T. Jaynes, and J. G. Miller, "General relationships between ultrasonic attenuation and dispersion," J. Acoust. Soc. Am. **63**(6), 1935–1937 (1978).
[27]K. R. Waters, J. Mobley, and J. G. Miller, "Causality-imposed (Kramers-Kronig) relationships between attenuation and dispersion," IEEE Trans. Ultrason., Ferroelectr., Freq. Control **52**(5), 822–823 (2005).
[28]A. Goldstein, D. R. Gandhi, and W. D. O'Brien, "Diffraction effects in hydrophone measurements," IEEE Trans. Ultrason., Ferroelectr., Freq. Control **45**(4), 972–979 (1998).
[29]E. G. Radulescu, P. A. Lewin, A. Goldstein, and A. Nowicki, "Hydrophone spatial averaging corrections from 1 to 40 MHz," IEEE Trans. Ultrason., Ferroelectr., Freq. Control **48**(6), 1575–1580 (2001).
[30]IEC 62127-3: *Ultrasonics—Hydrophones—Part 3: Properties of Hydrophones for Ultrasonic Fields up to 40 MHz* (International Electrotechnical Commission, Geneva, Switzerland, 2013).
[31]K. A. Wear, "Considerations for choosing sensitive element size for needle and fiber-optic hydrophones—Part I: Spatiotemporal transfer function and graphical guide," IEEE Trans. Ultrason., Ferroelectr., Freq. Control **66**(2), 318–339 (2019).